SECURITY CLASSIFICATION OF THIS PAGE (When Data Entered)

12

REPORT DOCUMENTATION PAGE

READ INSTRUCTIONS BEFORE COMPLETING FORM

1. REPORT NUMBER	2. GOVT ACCESSION NO.	3. RECIPIENT'S CATALOG NUMBER
3		

4. TITLE (and Subtitle)
Properties of UV-Cured Polyurethane Acrylates: Effect of Polyol Type and Molecular Weight

5. TYPE OF REPORT & PERIOD COVERED
Interim Technical Report

6. PERFORMING ORG. REPORT NUMBER

7. AUTHOR(s)
S.B. Lin, S.Y. Tsay, T.A. Speckhard, K.K.S. Hwang, J.J. Jezerc, and S.L. Cooper

8. CONTRACT OR GRANT NUMBER(s)
N00014-83-K-0423

9. PERFORMING ORGANIZATION NAME AND ADDRESS
University of Wisconsin
Department of Chemical Engineering
Madison, WI 53706

10. PROGRAM ELEMENT, PROJECT, TASK AREA & WORK UNIT NUMBERS

11. CONTROLLING OFFICE NAME AND ADDRESS
Office of Naval Research
Code 413
Arlington, VA 22217

12. REPORT DATE
June 20, 1984

13. NUMBER OF PAGES
44

14. MONITORING AGENCY NAME & ADDRESS(if different from Controlling Office)

15. SECURITY CLASS. (of this report)
Unclassified

15a. DECLASSIFICATION/DOWNGRADING SCHEDULE

16. DISTRIBUTION STATEMENT (of this Report)
Distribution unlimited

DISTRIBUTION STATEMENT A
Approved for public release
Distribution Unlimited

17. DISTRIBUTION STATEMENT (of the abstract entered in Block 20, if different from Report)

DTIC ELECTE JUL 18 1984 S D B

18. SUPPLEMENTARY NOTES
To be published in Chemical Engineering communications

19. KEY WORDS (Continue on reverse side if necessary and identify by block number)
Polyurethane, Acrylate, UV-cure, Polyol, Molecular weight

20. ABSTRACT (Continue on reverse side if necessary and identify by block number)
See accompanying abstract

DD FORM 1 JAN 73 1473 EDITION OF 1 NOV 65 IS OBSOLETE
S/N 0102-LF-014-6601

SECURITY CLASSIFICATION OF THIS PAGE (When Data Entered)

AD-A143 176

DTIC FILE COPY

84 07 12 016

Abstract

Several families of UV-cured polyurethane acrylates were synthesized and the effects of polyol type and molecular weight on their physical properties were investigated. Increasing polyol molecular weight led to a lower polyol glass transition temperature, a smaller amount of a separate urethane acrylate phase, and a larger chain length between crosslinks. The first two effects were reflected in lower modulus and strength at room temperature while the larger chain length between crosslinks led to higher elongation at break (room temperature) and lower modulus at high temperatures. The use of different polyols (polycarbonate, polytetramethylene oxide, polypropylene oxide, and polycaprolactone) primarily affected the room temperature modulus due to differences in the position and breadth of the polyol glass transition. The properties of materials based on isocyanatoethyl methacrylate (IEM) and toluene diisocyanate-2-hydroxyethyl methacrylate (TDI-HEMA) were also compared.

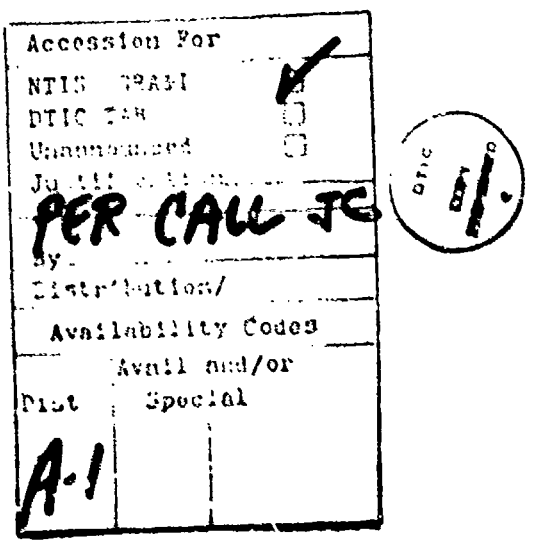

Properties of UV-Cured Polyurethane Acrylates: Effect of Polyol Type and Molecular Weight

Shaow B. Lin[a], S.Y. Tsay[b], T.A. Speckhard,

K.K.S. Hwang[c], J.J. Jezerc, and S.L. Cooper*

Department of Chemical Engineering
University of Wisconsin
Madison, WI 53706

JUNE 20, 1984

~~March 1984~~

[a] current address: R&D, Syntex Ophthalmics, Inc., Phoenix, AZ

[b] current address: Department of Chemical Engineering, National Cheung Kung University, Tainan, Taiwan, R.O.C.

[c] current address: Life Science Sector Laboratory, 3M Center, St. Paul, MN

* Author to whom correspondence should be addressed

I. INTRODUCTION

High intensity radiation from electron beams or ultraviolet sources has been shown to be an effective means to initiate polymerization in reactive oligomer systems (1-5). The advantages of this technology include higher throughput, savings in energy, and reduced or eliminated solvent emissions compared to solvent-based systems, since most formulations are 100% reactive oligomeric liquids (2). The major components of radiation curable systems are the reactive oligomer, reactive diluent, and photoinitiator. Other components which often appear in these systems include non-reactive modifiers, pigments, flow control additives, and plasticizers. The most important of these components in determining the mechanical properties is the reactive oligomer (2). Therefore, the molecular design of radiation sensitive oligomers has been a major concern in recent years.

Among commercially important candidates, acrylated urethanes are most often employed as oligomers because these materials combine the high abrasion resistance, toughness, high tear strength, and good low temperature properties of polyurethanes (6) with the superior optical properties and weatherability of polyacrylates. In general, a reactive mixture of urethane oligomer tipped with acrylic functionality is combined with vinyl monomers (reactive diluents) which are added to make harder products and/or to reduce the viscosity of the precursor liquid to obtain better processibility. Commercial urethane acrylate oligomers are normally prepared by a two step procedure. Typically, polyether or polyester macroglycols are sequentially tipped by an aromatic diisocyanate such as toluene diisocyanate (TDI), xylidine diisocyanate (XDI) or isophorone diisocyanate (IPDI), and then by 2-hydroxyethylacrylate (HEA) or 2-hydroxyethylmethacrylate (HEMA) (7-9). It is also possible to react the diisocyanate first with a deficiency of HEA or HEMA and then combine that adduct with the polyol. With and without combination of acrylate monomers, these systems are highly responsive to radiation, producing strong crosslinked films.

UV irradiation induced polymerization is accomplished by incorporation of suitable ketone type initiators usually in combination with accelerators or proton donors (10,11) which produce free radicals upon exposure to light of appropriate wavelength. This technology is now extensively used in the printing industry, where photoreproduction is possible, and in coating applications. Only recently, however, have any publications appeared describing the physical properties of urethane acrylates in any detail (2,12-20).

Oraby and Walsh (13,14) studied the mechanical properties of electron beam cured acrylated polyester urethanes based on TDI-HEA oligomers of varying oligomer structure, monomer content, and concentration of chain transfer agent. It was shown from stress-strain and thermal property measurements that increasing the molecular weight of the urethane acrylate from 1000 to 4600 resulted in a decrease in the stress at break, Young's modulus, and glass transition temperature, while the elongation at break increased. Based on dynamic mechanical and microscopic studies, Wadhwa and Walsh (15) concluded that these polyurethane acrylates have a one phase morphology in which hard segments and soft segments are homogeneously mixed. Wilkes and coworkers (16,17) investigated the effects of crosslink density on the morphology and mechanical properties of IPDI-HEA based materials. These materials were based on a crystallizable polycaprolactone polyol and possessed a spherulitic superstructure. Increased crosslinking reduced the degree of crystallinity and improved tensile strength.

Webb and coworkers (18,19) noted that the exposure of polyester urethane acrylates to humidity leads to a lowering of the glass transition temperature and a reduction of tensile properties relative to dry samples. The authors attributed these results to a replacement of interurethane and urethane-ester hydrogen bonds with hydrogen bonds to water molecules, Shilov et al. (20) investigated the heterogeneous structure of interpenetrating networks based on

polyurethane acrylates by small angle x-ray scattering.

In a previous publication from this laboratory (12) the properties of IPDI-HEA and TDI-HEA polytetramethylene oxide and polycaprolactone based materials were reported. Increasing soft segment molecular weight led to the development of a two phase morphology, reduced room temperature tensile strength and modulus, and increased elongation. No significant differences were noted between the tensile properties of IPDI and TDI based materials. One direct comparison between a polytetramethylene oxide and polycaprolactone based material indicated a slightly higher modulus but slightly lower ultimate properties for the polytetramethylene oxide based sample. The effects of reactive diluent monomer type and concentration were also investigated; those results will be compared with the results of recent studies of a similar nature in a forthcoming paper (21).

In this investigation radiation sensitive materials are described based on isocyanatoethyl methacrylate (IEM) and various polyols. IEM combines the acrylate and isocyanate functionality into one molecule thereby eliminating one step in the oligomer synthesis (22). Either functional group can react independently, usually without affecting the latent reactivity of the other group (22). Four series of materials have been prepared based on four different polyols (polycarbonate (CB), polypropylene oxide (PP), polytetramethylene oxide (ET), and polycaprolactone (ES)). In addition the polyol molecular weight was varied in some of the systems used. The effects of polyol type and molecular weight on the properties of IEM based UV-cured urethane acrylates were investigated using differential scanning calorimetry, dynamic mechanical spectroscopy, and tensile testing. The results for the IEM based materials were also compared with results for analogs derived from TDI-HEMA based materials.

II. EXPERIMENTAL

A. Materials

Isocyanatoethyl methacrylate (IEM) was kindly provided by M.R. Thomas of Dow Chemical and had a purity greater than 99% with 150 ppm of 2,6-di-t-butyl 4-methylphenol (ionol) inhibitor (22). It was used as received. Polycarbonate polyols (CB) (Vulkollan 2020) were received through the courtesy of Dr. H. Hespe of Bayer. Polypropylene oxide polyols (PP) and hydroxyethyl methacrylate (HEMA) were acquired from Aldrich Chemical Co. Polytetramethylene oxide (ET) and polycaprolactone (ES) polyols were obtained from Quaker Oats Chemical Co. and Polysciences respectively. These materials were used after vacuum dehydration for at least one day. Toluene diisocyanate (20/80 mixture of 2,6 and 2,4 isomers) (TDI) was used as received from BASF Wyandotte.

IEM based UV-curable urethane acrylate oligomers were synthesized by slowly adding one mole of dehydrated polyol into a nitrogen-purged reaction flask containing two moles of IEM. The temperature was kept below 45°C to avoid thermal polymerization of vinyl groups. About .15 wt.% stannous octoate (M and T Chemicals) was added and two hours were allowed to complete the reaction. 100 ppm of hydroquinone was added as an inhibitor to ensure stable shelf life before UV-curing. The IEM-polyol structure shown in Figure 1 was confirmed by Fourier transform infrared spectroscopy.

A procedure similar to that described previously (12) was used to synthesize TDI based urethane acrylates. An equimolar amount of dehydrated HEMA was added dropwise to TDI under a nitrogen atmosphere. Again, the temperature was kept below 45°C to avoid thermal polymerization of the vinyl groups. In this case the desired product is HEMA-TDI; however, some HEMA-TDI-HEMA and free TDI are produced. The dominant product should be HEMA-TDI due to the reduced reactivity of the second isocyanate of the non-symmetric 2,4 TDI isomer (23,24). When the TDI/HEMA reaction mixture temperature started to drop, a stoichiometric

quantity of dehydrated polyol was added along with stannous octoate catalyst. The mixture was agitated for two hours and heated to 70°C to complete the reaction. The structure of the dominant product is shown in Figure 1.

The photoinitiator used was a one-to-one mixture of 2,2'-diethoxyacetophenone (Polysciences) and N-methyldiethanolamine (Aldrich). Approximately .6 wt% of the initiator mixture was added to the urethane acrylate oligomer prior to curing. The reactive diluent chosen in this study was N-vinylpyrrolidone (NVP) (Aldrich).

The structure of the IEM based urethane acrylates was varied by changing the polyol type and the polyol molecular weight. Several TDI-HEMA based materials were prepared to investigate possible differences between IEM and TDI based samples and to note whether similar effects of polyol type and molecular weight are observed. All of the materials studied are listed in Table 1. Sample designation codes indicate whether the sample is IEM or TDI-HEMA (T) based, the polyol type and molecular weight, and the weight percent of NVP added before curing (0 or 25%). For example, IEM-ET1000-25N indicates a 1000 molecular weight polytetramethylene oxide, IEM based material with 25 weight percent NVP.

B. Sample Preparation

The mixture of urethane acrylate oligomer, 0.6 wt% photoinitiator and reactive diluent (NVP) was heated slightly above ambient temperature to ensure homogeneous mixing. The liquid prepolymers were poured into teflon coated molds of varied thickness. Samples were about 0.2-0.3 mm in thickness for tensile specimens and 50 μm for dynamic mechanical analysis. To perform kinetic studies prepolymers were also cast directly on KBr plates with a thickness that allowed at least 30% transmission before and after UV-curing.

The samples were irradiated from one side under a nitrogen atmosphere using a bank of 20W mercury lamps (λ = 365 nm) as the irradiation source. An irra-

diation time of 10 minutes was found to cure specimens satisfactorily and was used for all of the samples.

C. Characterization Methods

1. Viscometry

The viscosity of prepolymers was characterized using a Brookfield viscometer. Some polycarbonate based prepolymers were solid at ambient temperature; therefore, for comparison purposes, all viscosity measurements were performed at 40°C.

2. Soxhlet Extraction

The gel fraction of the cured samples was determined by Soxhlet extraction using toluene for 24 hours. The insoluble gel fraction was dried under vacuum for about two days and weighed to determine the gel fraction.

3. Infrared Spectroscopic Measurements

Infrared spectra of thin polymer films cast on KBr plates were taken before and after UV irradiation using a Nicolet 7199 Fourier-transform infrared spectrometer. The characteristic C=C absorption of urethane acrylate at 1635 cm^{-1} was used to determine the extent of photoinitiated vinyl polymerization. The N=C=O stretching near 2270 cm^{-1} was used to monitor the extent of reaction in prepolymer preparations.

4. Stress-Strain Measurements

Uniaxial stress-strain measurements at room temperature were made using a table model Instron tensile testing machine with a crosshead speed of 0.5 inch/min. Dumbbell shaped film samples with a gauge length of 1.5 inch were stamped out with an ASTM 412 die. The engineering stress was calculated as the ratio of force to initial cross-sectional area. Reported data were the average of three tests.

5. Dynamic Mechanical Measurements

Dynamic mechanical data were collected at 110 Hz using a Toyo Rheovibron

DDV-IIC apparatus which was controlled automatically by a LSI-11/03 microprocessor. Film samples of about 20 x 2 x 0.05 mm were tested under a nitrogen blanket from -150°C to 200°C at a heating rate of 2°C/min.

6. Differential Scanning Calorimetry

DSC thermograms of urethane acrylate prepolymers as well as the UV-cured polymers were recorded using a Perkin-Elmer DSC-II equipped with a thermal analysis data station. The experiments were carried out from -120°C to 180°C at a heating rate of 20°C/min under a helium purge. The DSC thermograms were normalized to equivalent sample weight to facilitate comparisons.

III. RESULTS AND DISCUSSION

A. Viscosity of Urethane Acrylate Prepolymers

The viscosity of solvent-free prepolymers in coating and printing applications is considered of primary importance. The measured viscosity at 40°C of selected prepolymers is shown in Table 2. The data in Table 2 show that IEM based prepolymers have lower bulk viscosities than corresponding TDI-HEMA based samples by at least an order of magnitude. As expected (4), addition of NVP (data not shown) led to a large reduction in the viscosity of both IEM and TDI based materials. Table 2 also shows that increasing polyol molecular weight and using polytetramethylene oxide polyol instead of polypropylene oxide polyol leads to an increase in the prepolymer viscosity for both IEM and TDI based samples.

B. The Extent of Photopolymerization

The UV-initiated polymerization process was monitored by infrared spectroscopy as illustrated in Figure 2 where the infrared spectrum of IEM-ET2000-0 was taken prior to and after one minute of UV irradiation. The twice expanded difference (after - before) spectrum is plotted to show spectroscopic changes resulting from the curing process. The complete disappearance of the C=C band at 1635 cm^{-1} indicates that the vinyl polymerization reaction has occurred. The

differences in the spectra at 1164 cm^{-1} and near 1300 cm^{-1} are typical of carbonyl and methyl groups linked to vinyl groups that have reacted. The shift of the carbonyl stretching at 1720 cm^{-1} may be indicative of side reactions associated with the acrylate carbonyl (12). Beachell et al. (25,26) reported on the gradual UV-induced decomposition of urethane compounds. In the present case, minimal changes in the spectral regions where urethane decomposition products absorb indicate urethane stability during the photopolymerization. Thus the primary photochemical reaction is polymerization of the vinyl groups. Compared with the TDI-HEA based systems studied previously (12) these IEM based materials exhibited a higher rate of UV-curing. This result is attributed to the lower viscosity of the IEM based prepolymers and the fact that gelation occurred at a higher conversion of vinyl groups in samples based on IEM.

The extent of photopolymerization was also measured by Soxhlet extraction to determine the gel fraction; results for selected samples are shown in Table 3. Generally, samples were found to contain greater than .95 gel fraction although lower values were occasionally found presumably due to inhibition of the polymerization by dissolved oxygen. Only samples with a gel fraction greater than .95 were used in the structure-property studies.

C. Thermal Properties

Differential scanning calorimetry (DSC) thermograms for several families of materials are shown in Figures 3 and 5-7. Glass transition temperatures determined from the thermograms are listed in Table 1. Figure 3 shows DSC curves for the IEM-PP-0 series before (broken line) and after (solid line) UV-curing. The glass transition temperature for these samples and the corresponding UV-cured materials with 25 wt% NVP are plotted as a function of molecular weight in Figure 4. Figures 3 and 4 show that the uncured, 0 wt% NVP materials exhibit a trend of increasing glass transition temperature with decreasing polyol molecular weight. In contrast, low molecular weight polymers generally exhibit

decreasing Tg with decreasing polyol molecular weight which is interpreted as an increase in the free volume associated with chain ends leading to increased chain mobility (27,28). However, similar trends of increasing glass transition temperature with decreasing polyol molecular weight are commonly observed for polyurethane block copolymers and are attributed to decreases in free volume and mobility due to the bonding of the polyol segments to the rigid urethane blocks (27,28). UV-curing of the 0 wt% NVP samples leads to an increase in the glass transition temperature that is attributed to a reduction in the mobility of the polyol chains due to crosslinking. This effect is particularly noticeable at lower polyol molecular weights due to the increasing influence of chain end restrictions as the polyol chain length decreases (27,28).

Figures 3 and 4 also show that the incorporation of 25 wt% NVP leads to materials (after UV-curing) with higher glass transition temperatures. This could be due to an increased crosslinking effect but is more likely a result of adding a high glass transition temperature component to the materials. (The glass transition temperature of poly(N-vinylpyrrolidone) has been measured by DSC to be 73°C (12)). The fact that the Tg versus polyol molecular weight curves for the 0 and 25 wt% NVP materials are similar indicates that adding NVP does not promote increased restrictions of the polyol chains due to increased crosslinking. If that were indeed the case, the effect, as noted above, would be expected to be greater at low polyol molecular weights leading to a difference in the Tg versus polyol molecular weight curve shapes similar to the differences between the before and after UV-curing IEM-PP-0 curve shapes. The effect of adding NVP and other reactive diluents on the glass transition temperatures of UV-curable urethane acrylates will be investigated further in a forthcoming publication (21).

Figure 5 again shows the trend of increasing glass transition temperature with decreasing polyol molecular weight, in this case for the IEM-ES-25N-series

materials. Here also the effect is more noticeable at low polyol molecular weights. The effect of polyol type at roughly comparable polyol molecular weights can be seen in Figure 6. The polycarbonate (CB) based sample has the highest Tg followed by the polycaprolactone (ES) and polypropylene oxide (PP) based materials with the polytetramethylene-oxide based sample having the lowest glass transition temperature. This trend is consistent with the chain flexibility of the various polyols, polycarbonate having the stiffest chain backbone and polytetramethylene oxide the most flexible.

The data in Figure 7 allow for comparison of the thermal properties of IEM and TDI-HEMA based materials. The data in Figure 7 indicate that, at least for polypropylene oxide and polytetramethylene-oxide based samples, TDI-HEMA based materials possess a higher glass transition temperature. Similar TDI-HEA based materials (12) also have a higher Tg than the IEM based samples. The higher glass transition temperatures of the TDI based materials can be attributed to the stiffer, aromatic structure of TDI compared with the more flexible, aliphatic structure of IEM (Figure 1). In a previous study of TDI-HEA based materials (12) several samples based on 2000 molecular weight polytetramethylene oxide exhibited in DSC thermograms a second, high temperature glass transition associated with the development of a separate urethane acrylate and reactive diluent phase in the material. None of the samples in this study exhibited similar behavior. However, this does not necessarily eliminate the possibility of phase separation in these materials since it was noted previously that several materials exhibiting two phase behavior in dynamic mechanical spectroscopy experiments did not exhibit two distinct glass transitions in their DSC thermograms. In fact, the authors (12) noted that no distinct glass transition was observed by DSC for several materials that were shown by dynamic mechanical spectroscopy to possess one very broad glass transition, implying some heterogeneity in the material. Similar behavior was exhibited by some samples in this

study (for example, sample IEM-ES530-25N in Figure 5). The possibility of a two phase microstructure existing in these materials will be discussed further in light of results from dynamic mechanical spectroscopy experiments.

The polytetramethylene oxide, polycarbonate and polycaprolactone based materials might be expected to exhibit crystallization and or melting behavior since these polyols are capable of crystallizing as high molecular weight homopolymers, yet no crystallization exotherms or melting endotherms were observed for any of the samples. This can partially be attributed to the low molecular weight of the polyols used; however, 2000 molecular weight polycaprolactone and polytetramethylene oxide based polyurethane block copolymers have been found to exhibit soft segment crystallization (29). Van Bogart et al. (29) have noted that increased mixing of hard (urethane) and soft (polyol) segments in polyurethane block copolymers reduces the amount of both hard and soft segment crystallinity. In this study, no evidence for a two phase structure was observed by DSC; however, as will be discussed in the next section, some degree of phase separation may exist. Yet similar 2000 molecular weight polytetramethylene oxide based UV-cured urethane acrylates that do exhibit phase separation by DSC (two glass transition temperatures) did not exhibit polyol crystallinity (12). Therefore, in addition to low polyol molecular weight, restrictions on polyol mobility due to crosslinking are probably responsible for the lack of polyol crystallinity to a greater extent than interactions between the polyol and the urethane acrylate or reactive diluent.

D. Mechanical Properties

Stress-strain curves for several series of materials are shown in Figures 8, 11, 13, 14, and 16, and tensile properties (Young's modulus, elongation at break, and stress at break) are listed in Table 1. Dynamic mechanical storage modulus and loss factor curves are shown for several families of the UV-cured urethane acrylates in Figures 10, 12, 15, and 17. Figure 8 displays stress-

strain curves for the IEM-PP series materials, and tensile properties as a function of polypropylene oxide molecular weight are plotted for the IEM-PP-25N materials in Figure 9. Figure 9 shows that Young's modulus decreases with increasing polyol molecular weight while the elongation at break increases; similar trends with polyol molecular weight have been observed by Oraby and Walsh (13). The decrease in modulus with polyol molecular weight for the IEM-PP-25N materials closely parallels the decrease in glass transition temperature with polyol molecular weight (Figure 4). Decreasing modulus and increasing elongation at break are generally associated with a decreasing glass transition temperature since more flexible materials are usually weaker but less brittle. Increasing polyol molecular weight also results in an increase in chain length between crosslinks. This effective reduction of the crosslink density would also be expected to give rise to a lower modulus but greater elongation. It is also interesting to note that the stress at break which is affected by both the brittleness and strength of a material exhibits a shallow minimum with increasing polyol molecular weight (Figure 9).

Figure 8 shows that the IEM-PP-0 series materials exhibit the same trends of tensile properties with molecular weight as the IEM-PP-25N samples. A comparison of samples from the two series at the same polyol molecular weight shows that adding 25 wt% NVP dramatically improves elongation and stress at break while increasing the modulus slightly. Generally, the incorporation of NVP in UV-curable urethane acrylate results in a larger increase in modulus than that observed for the IEM-PP1000 and IEM-PP2000 samples (12). The effect of reactive diluent content on the morphology and properties of UV-cured urethane acrylates will be discussed in detail in a subsequent publication (21).

The dynamic mechanical storage modulus and loss modulus curves for the IEM-ES-25N series materials are shown in Figure 10. The loss modulus curves exhibit peaks at approximately -120°C and -40°C and a high temperature peak or

shoulder at about 50°C. The peak at -120°C is attributed to localized motion of the polycaprolactone segments (6) while the peak at about -40°C is associated with the glass transition of the polyol segments that was also noted in the DSC data (Figure 5). In accord with the DSC data, decreasing polyol molecular weight leads to a higher polyol glass transition temperature. Decreasing polyol molecular weight also results in an increasing weight fraction of urethane acrylate segments and leads to development of a separate phase as indicated by growth of a high temperature shoulder in the loss modulus curve. No associated high temperature transition was seen in the DSC data; however, as discussed previously, this is not unusual (12,27,30). Figure 10 also shows that decreasing polyol molecular weight leads to an increase in the storage modulus in both the transition and in the high temperature rubbery region. The increase of the storage modulus in the transition region is primarily due to an increasing polyol glass transition temperature which effectively shifts the storage modulus curve to higher temperature. Thus at a given temperature the higher glass transition temperature material has a greater modulus. The increased fraction of a separate urethane acrylate/reactive diluent phase with decreasing polyol molecular weight will also increase the storage modulus in the transition region. The increase of the modulus with polyol weight at temperatures above 100°C is primarily due to the increase in crosslink density with shorter (lower molecular weight) polyol chains. The stress-strain curves for the IEM-ES-25N series materials are shown in Figure 11. Similar trends with polyol molecular weight for this series are attributable to the same morphological factors which were suggested to explain the behavior of the IEM-PP materials. Figure 11 and Table 1 also demonstrate relative changes in Young's modulus with polyol molecular weight that are in good agreement with the dynamic storage modulus data at room temperature (Figure 10).

Dynamic mechanical storage modulus and loss factor (tan δ) curves are shown

for various IEM-polyol-0 materials with comparable polyol molecular weights in Figure 12. The loss factor curves exhibit one major peak associated with the polyol glass transition that is broadened or has a shoulder on the high temperature side indicative of the development of a urethane acrylate phase. If the peak in the loss factor curve is taken as a relative measure of the glass transition temperature, the trend of glass transition temperature with polyol type (CB>ES>PP>ET) noted in the DSC curves is observed. The storage modulus curves show differences in the transition region that reflect the position and breadth of the polyol glass transition. The storage modulus at high temperatures is roughly the same for all of the materials. Stress-strain curves for the same family of materials (except IEM-ES830-0 is substituted for IEM-ES1250-0) are shown in Figure 13. The polycaprolactone (ES) and polycarbonate (CB) based materials exhibit superior ultimate properties while the trend of Young's modulus with polyol type (CB>ET>ES>PP) parallels the trend in the dynamic storage modulus at 25°C. As noted above, both the position and breadth of the polyol glass transition influence the room temperature modulus. For example, the polytetramethylene oxide sample (IEM-ET1000-0) has a glass transition that is centered at a lower temperature than the corresponding ES or PP samples, but its transition is broader leading to a higher room temperature modulus.

Incorporating 25 wt% NVP accentuates the differences in tensile properties of the various polyol types as shown in Figure 14. The differences in Young's modulus follow the same trend with polyol type noted above and again are reflected in the room temperature dynamic storage modulus data shown in Figure 15. Figure 15 also demonstrates that incorporating 25 wt% NVP enhances the development of a second, high glass transition temperature phase in the samples by the growth of the high temperature peak or shoulder in the loss factor curves. The addition of NVP also gives rise to an increase in the polyol glass transition temperature. As noted above, both of these effects increase the dynamic

storage modulus in the transition region and are also reflected in the improvement of the Young's modulus that can be seen by comparing the data in Figures 13 and 14.

Stress-strain curves for several IEM and corresponding TDI-HEMA based materials are shown in Figure 16. In all cases the TDI-HEMA based materials exhibit a much greater modulus and stress at break and slightly improved elongation at break. The effects of polyol type (polytetramethylene oxide or polypropylene oxide) and polyol molecular weight (1000 or 2000) on the tensile properites follow the same trends discussed previously for both the IEM and TDI-HEMA based materials. The improved tensile strength and modulus of the TDI-HEMA based materials compared with the IEM based samples is also reflected in the transiton region storage modulus data shown in Figure 17. The loss factor curves in Figure 17 indicate that the increase in the storage modulus in the transition region of the TDI-HEMA samples relative to IEM based analogs is due to an increase in the polyol glass transition temperature (note also the DSC data in Figure 7) and an increased amount of the urethane acrylate phase. Both of these effects could be anticipated on the basis of the differences in the chemical structure of the TDI-HEMA and IEM components (Figure 1). As noted previously, TDI, because of its aromatic nature, would be expected to lead to a higher glass transition temperature when it is reacted with a polyol. Also, TDI-HEMA based materials contain a greater weight fraction of the urethane acrylate component and the TDI-HEMA component is probably less compatible with the polyether polyols than the aliphatic IEM structure. Both of these factors lead to a greater amount of urethane acrylate phase in TDI-HEMA based materials compared with IEM based samples.

IV. SUMMARY

The effects of polyol type and molecular weight on the properties of UV-cured polyurethane acrylates have been investigated using differential

scanning calorimetry, dynamic mechanical spectroscopy and tensile testing. Increasing polyol molecular weight led to a lower polyol glass transition temperature, a smaller amount of a separate urethane acrylate phase, and a longer chain length between crosslinks. The first two effects were reflected in lower dynamic and tensile moduli and tensile strength at room temperature. The longer chain length between crosslinks was manifested in higher elongations at break (room temperature) and a lower dynamic storage modulus at high temperatures. The effect of polyol type was primarily associated with the position and breadth of the polyol glass transition. The dynamic storage and tensile moduli at room temperature were found to increase with different polyols in the order polycarbonate > polytetramethylene oxide > polycaprolactone > polypropylene oxide. Differences in the polyols did not significantly affect the elongation at break or the dynamic storage modulus at high temperatures.

A comparison of several IEM and corresponding TDI-HEMA based samples showed that the TDI-HEMA based materials possessed a higher polyol glass transition temperature and a larger weight fraction of phase separated urethane acrylate material. These differences were correlated with the differences in chemical structure between IEM and TDI-HEMA and resulted in greater tensile strength, modulus and dynamic storage modulus in the transition region in TDI-HEMA based materials. IEM and TDI-HEMA based samples exhibited similar trends with polyol type and molecular weight. The bulk viscosity of IEM based materials before UV-curing was found to be an order of magnitude lower than the viscosity of TDI-HEMA based analogs.

Acknowledgements:

The authors would like to thank M. R. Thomas of Dow Chemical Co. for supplying the IEM and Dr. H. Hespe of Bayer for providing the polycarbonate diols. The authors acknowledge partial support of this research by the Office of Naval Research and the Naval Air Systems Command.

REFERENCES

1. W. Mareau and N. Viswanathan, ACS Org. Coat. Preprints, 35(1), 108 (1975).

2. C. S. Schmiole, J. Coated Fabrics, 8, 10 (1978).

3. J. V. Crivello, ACS Org. Coat. Preprints, 41, 560 (1979).

4. L. Kushner and R. S. Tu, Modern Plastics, 87 (1983).

5. C. Decker, ACS Polym. Matl. Preprints, 49, 32 (1983).

6. A. Lilaonitkul and S. L. Cooper, "Advances in Urethane Science and Technology", K. C. Frisch and S. L. Reegen, Eds., Technomic Publ. Co., 7, 163 (1979).

7. Nippon Kokai Tokkyo Koho, 48-43657 (1973) (Japanese Patent).

8. Nippon Kokai Tokkyo Koho, 46-29525 (1971) (Japanese Patent).

9. U.S. Patent Number 3,907,865 (1975).

10. U.S. Patent Number 2,993,789 (1961).

11. T. Higuchi, in "Photopolymer" edited by T. Tsunoda (CMC, Tokyo, 1977) p. 137.

12. M. Koshiba, K. K. S. Hwang, S. K. Foley, D. J. Yarusso, and S. L. Cooper, J. Materials Sci., 17, 1447 (1982).

13. W. Oraby and W. K. Walsh, J. Applied Polym. Sci., 23, 3227 (1979).

14. W. Oraby and W. K. Walsh, J. Applied Polym. Sci., 23, 3243 (1979).

15. L. H. Wadhwa and W. K. Walsh, ACS Org. Coat. Preprints, 42, 509 (1980).

16. K. Park and G. L. Wilkes, ACS Org. Coat. Preprints, 41, 308 (1979).

17. E. G. Joseph, G. L. Wilkes and K. Park, ACS Polymer Preprints, 20, 520 (1979).

18. D. A. Bolon, G. M. Lucas, D. R. Olson, and K. K. Webb, J. Appl. Polym. Sci., 25, 543 (1980).

19. D. R. Olson and K. K. Webb, ACS Org. Coat. Preprints, 39, 518 (1978).

20. V. V. Shilor, Yu. S. Lipatov, L. V. Karabanova and L. M. Sergeeva, J. Polym. Sci. Polym. Chem. Ed., 17, 3083 (1979).

21. T. A. Speckhard, K. K. S. Hwang, S. B. Lin, S. Y. Tsay, M. Koshiba, Y. S. Ding, and S. L. Cooper, submitted for publication.

22. M. R. Thomas, ACS Org. Coat. Preprints, 46, 506 (1982).

23. L. L. Ferstandig and R. A. Scherrer, J. Am. Chem. Soc., 81, 4838 (1959).

24. F. H. Brock, J. Org. Chem., 24, 1802 (1959).

25. H. C. Beachell, and I. L. Chang, J. Polym. Sci., Part A-1, 10, 503 (1972).

26. H. C. Beachell, and C. P. Ngocson, J. Appl. Polym. Sci., 7, 2217 (1963).

27. T. A. Speckhard, P. E. Gibson, S. L. Cooper, V. S. C. Chang, and J. P. Kennedy, submitted to Polymer.

28. D. Z. Zdrahala, S. L. Hager, R. . Gerkin, and F. E. Critchfield, J. Elast. and Plast., 12, 225 (1980).

29. J. W. C. Van Bogart, D. A. Bluemke, and S. L. Cooper, Polymer, 22, 1428 (1981).

TABLE 1

SAMPLE DESIGNATION, TENSILE PROPERTIES AND GLASS TRANSITION TEMPERATURE OF UV-CURED URETHANE ACRYLATES

SAMPLE DESIGNATION	YOUNG'S MODULUS (MPa)	ELONGATION AT BREAK (%)	STRESS AT BREAK (MPa)	DSC T_g (°C)
IEM-PP1000-0	10.7	17	1.8	-37
IEM-PP1000-25N	10.5	34	3.2	-35
IEM-PP2000-0	6.0	28	1.6	-54
IEM-PP2000-25N	6.0	48	2.3	-50
IEM-PP3000-0	4.5	27	1.1	-58
IEM-PP3000-25N	5.2	65	2.4	-56
IEM-PP4000-0	2.9	66	1.6	-62
IEM-PP4000-25N	4.2	115	2.9	-58
IEM-ET1000-0	9.5	19	1.8	-59
IEM-ET1000-25N	14.1	42	4.4	-57
IEM-ET2000-25N	6.0	80	4.1	—
IEM-ES530-25N	61.5	40	11.3	-5
IEM-ES830-0	9.0	38	3.1	-38
IEM-ES830-25N	20.5	58	7.4	-34
IEM-ES1250-0	-	17	2.4	—
IEM-ES1250-25N	11.9	48	3.6	-53
IEM-ES1970-25N	8.0	72	3.0	-55
IEM-CB590-0	46.2	30	8.9	2
IEM-CB1020-0	13.9	25	3.2	-11
IEM-CB1020-25N	30.	63	9.3	25
IEM-CB1970-0	6.1	44	2.3	-39
T-PP1000-0	—	—	—	-33
T-PP1000-25N	101.	44	11.2	-
T-PP2000-25N	47.7	87	7.4	-
T-ET1000-0	34.4	57	13.7	-48
T-ET1000-25N	128.	93	20.1	-47
T-ET2000-25N	80.	136	12.	—

Table 2. Viscosity of Selected Urethane ...rylate Prepolymers

Sample	Viscosity (centipose)
IEM-PP1000	460
IEM-PP2000	530
IEM-PP3000	550
IEM-PP4000	1030
IEM-ET1000	690
IEM-ET2000	1860
T-PP1000	4,850
T-PP2000	10,140

Table 3 Gel Fractions of UV-Cured Urethane Acrylates

Sample	Gel Fraction (%)
IEM-PP1000-25N	98.9
IEM-ET1000-25N	98.5
IEM-ET2000-25N	96.9
IEM-CB1020-25N	99.1
T-ET1000-25N	98.8
T-ET2000-25N	96.0

FIGURE CAPTIONS

Figure 1. Chemical structure of UV-curable urethane acrylate components and prepolymers.

Figure 2. Infrared absorbance spectrum of sample IEM-ET2000-0 before UV-curing and twice expanded difference spectrum of the same sample before and after one minute of UV-curing.

Figure 3. DSC thermograms of the IEM-PP-0 series materials before (---) and after (——) UV-curing.

Figure 4. DSC glass transition temperature versus polypropylene oxide molecular weight for the IEM-PP series materials.

Figure 5. DSC thermograms of the IEM-ES-25N series materials.

Figure 6. DSC thermograms of IEM-polyol-0 materials.

Figure 7. DSC thermograms for corresponding IEM and TDI-HEMA based materials.

Figure 8. Stress-strain curves for the IEM-PP-0 (——) and IEM-PP-25N (---) series materials.

Figure 9. Young's modulus (O,Y), stress at break (•,σ_b), and elongation at break (O,ϵ_b) as a function of polyol molecular weight for the IEM-PP-25N series materials.

Figure 10. Dynamic mechanical storage (E') and loss modulus (E") curves for the IEM-ES-25N series materials.

Figure 11. Stress-strain curves for the IEM-ES-25N series materials.

Figure 12. Dynamic mechanical storage modulus (E') and loss factor (tan δ) curves for IEM-polyol-0 materials.

Figure 13. Stress-strain curves for IEM-polyol-0 materials.

Figure 14. Stress-strain curves for IEM-polyol-25N materials.

Figure 15. Dynamic mechanical storage modulus (E') and loss factor (tan δ) curves for IEM-polyol-25N materials.

Figure 16. Stress-strain curves for corresponding IEM and TDI-HEMA based materials.

Figure 17. Dynamic mechanical storage modulus (E') and loss factor (tan δ) curves for corresponding IEM and TDI-HEMA based materials.

URETHANE OLIGOMER COMPONENT STRUCTURES

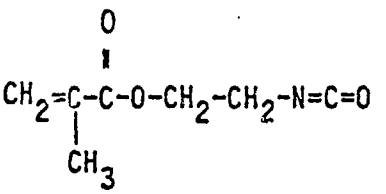

isocyanatoethyl methacrylate (IEM)

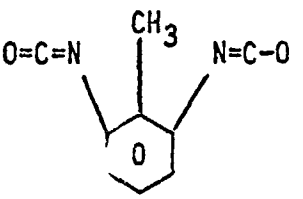

2,6-toluene diisocyanate (T)

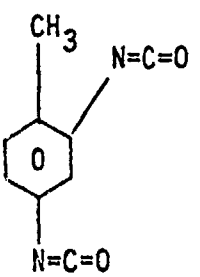

2,4-toluene diisocyanate (T)

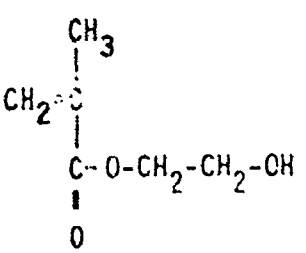

2-hydroxyethyl methacrylate (HEMA)

Chemical Structures

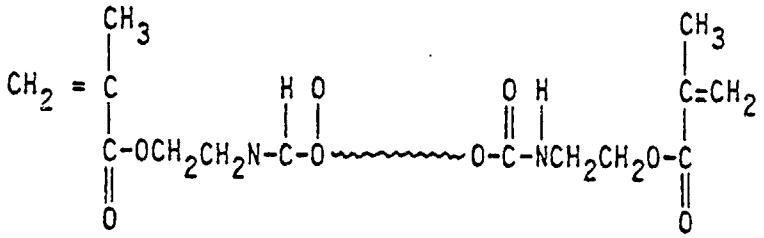

IEM-POLYOL-IEM

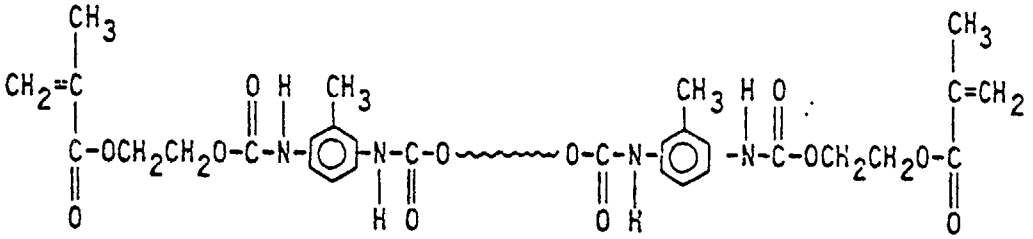

HEMA-TDI-POLYOL-TDI-HEMA

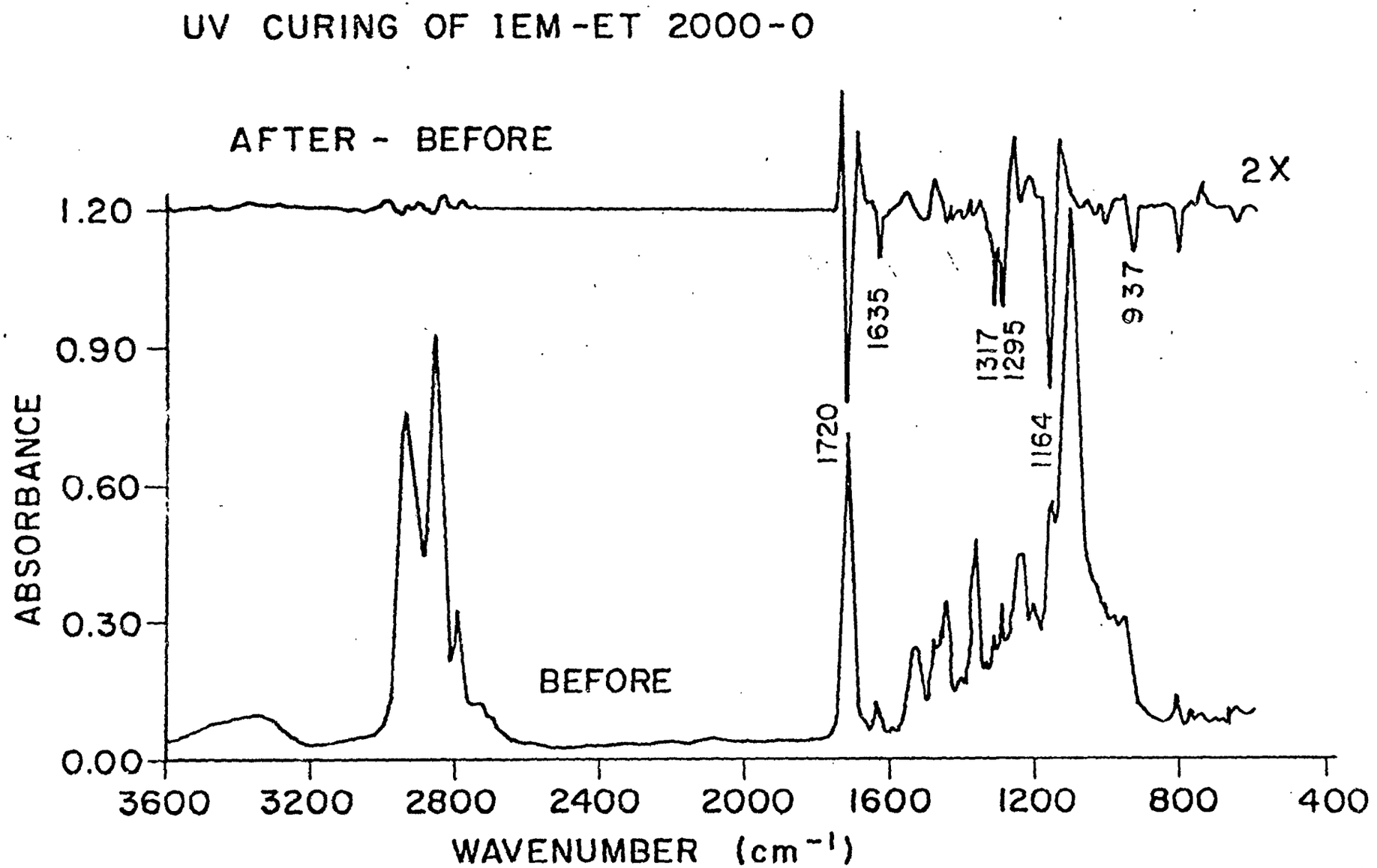
UV CURING OF IEM-ET 2000-O
AFTER - BEFORE
2X
1.20
0.90
0.60
0.30
0.00
ABSORBANCE
1720
1635
1317
1295
1164
937
BEFORE
3600
3200
2800
2400
2000
1600
1200
800
400
WAVENUMBER (cm⁻¹)

FIG 2.

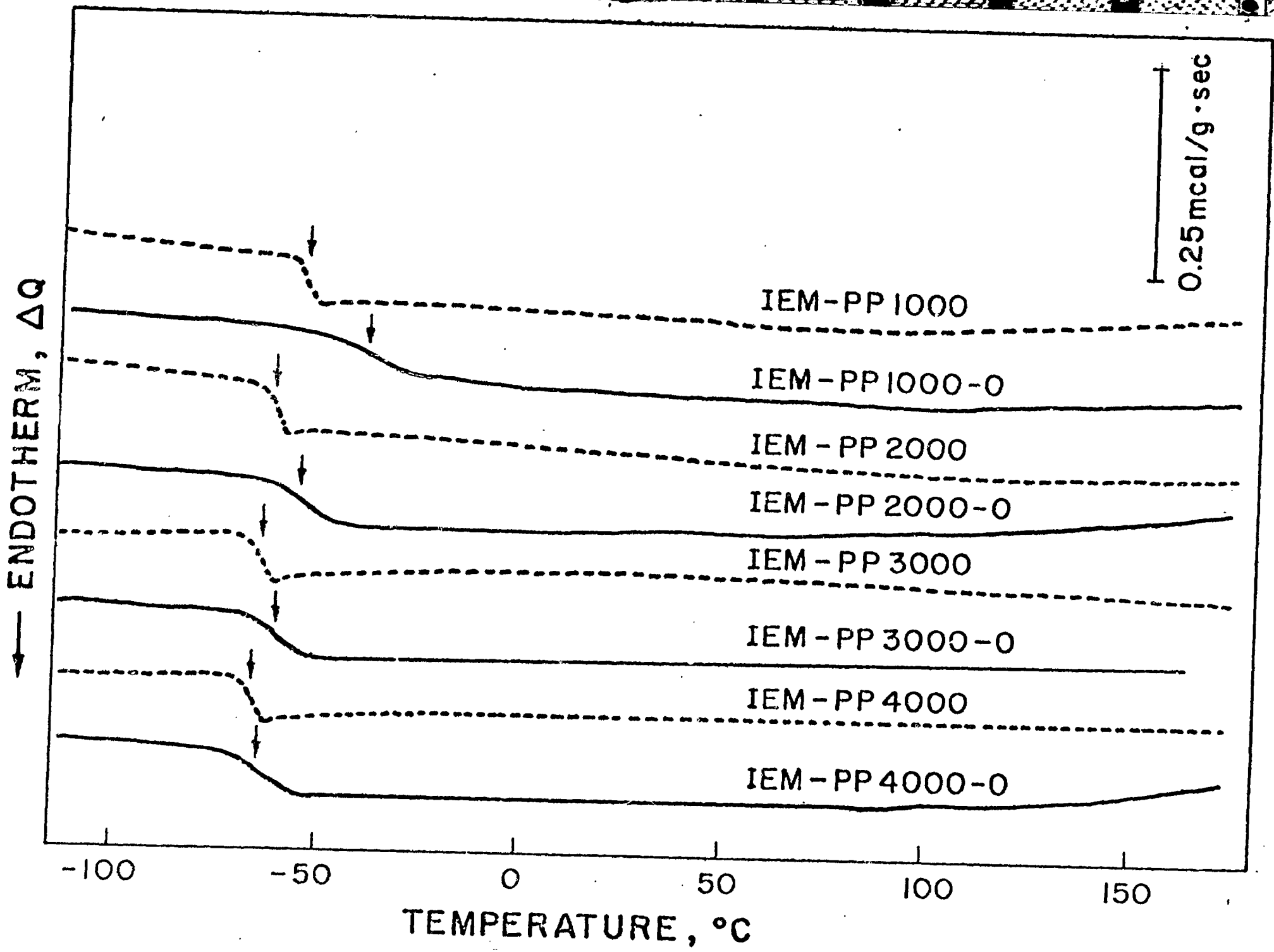
0.25 mcal/g·sec
IEM-PP 1000
IEM-PP 1000-0
IEM-PP 2000
IEM-PP 2000-0
IEM-PP 3000
IEM-PP 3000-0
IEM-PP 4000
IEM-PP 4000-0
↓ ENDOTHERM, ΔQ
-100
-50
0
50
100
150
TEMPERATURE, °C

FIG 3

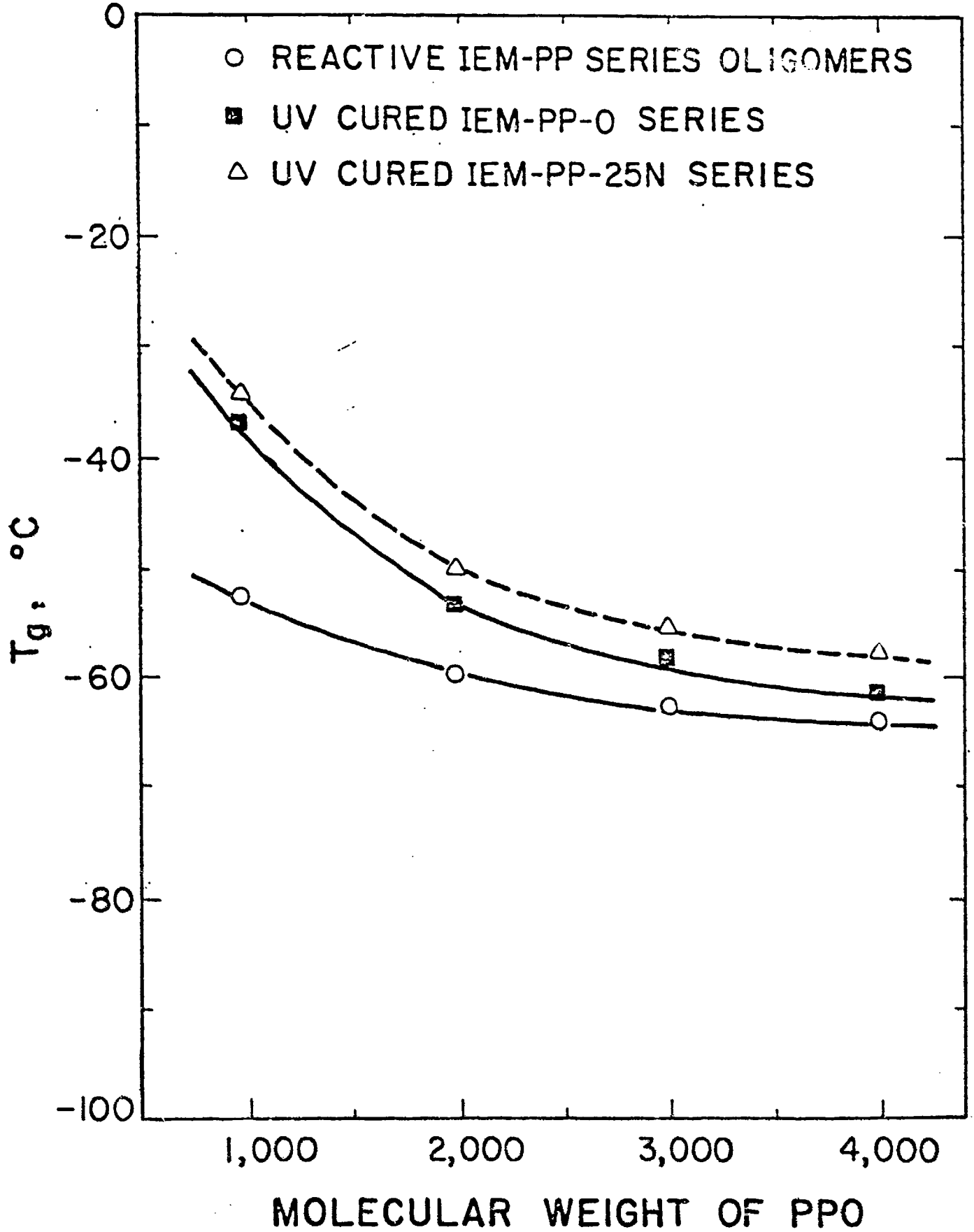
REACTIVE IEM-PP SERIES OLIGOMERS
UV CURED IEM-PP-0 SERIES
UV CURED IEM-PP-25N SERIES
0
-20
-40
-60
-80
-100
Tg, °C
1,000
2,000
3,000
4,000
MOLECULAR WEIGHT OF PPO

FIG 4

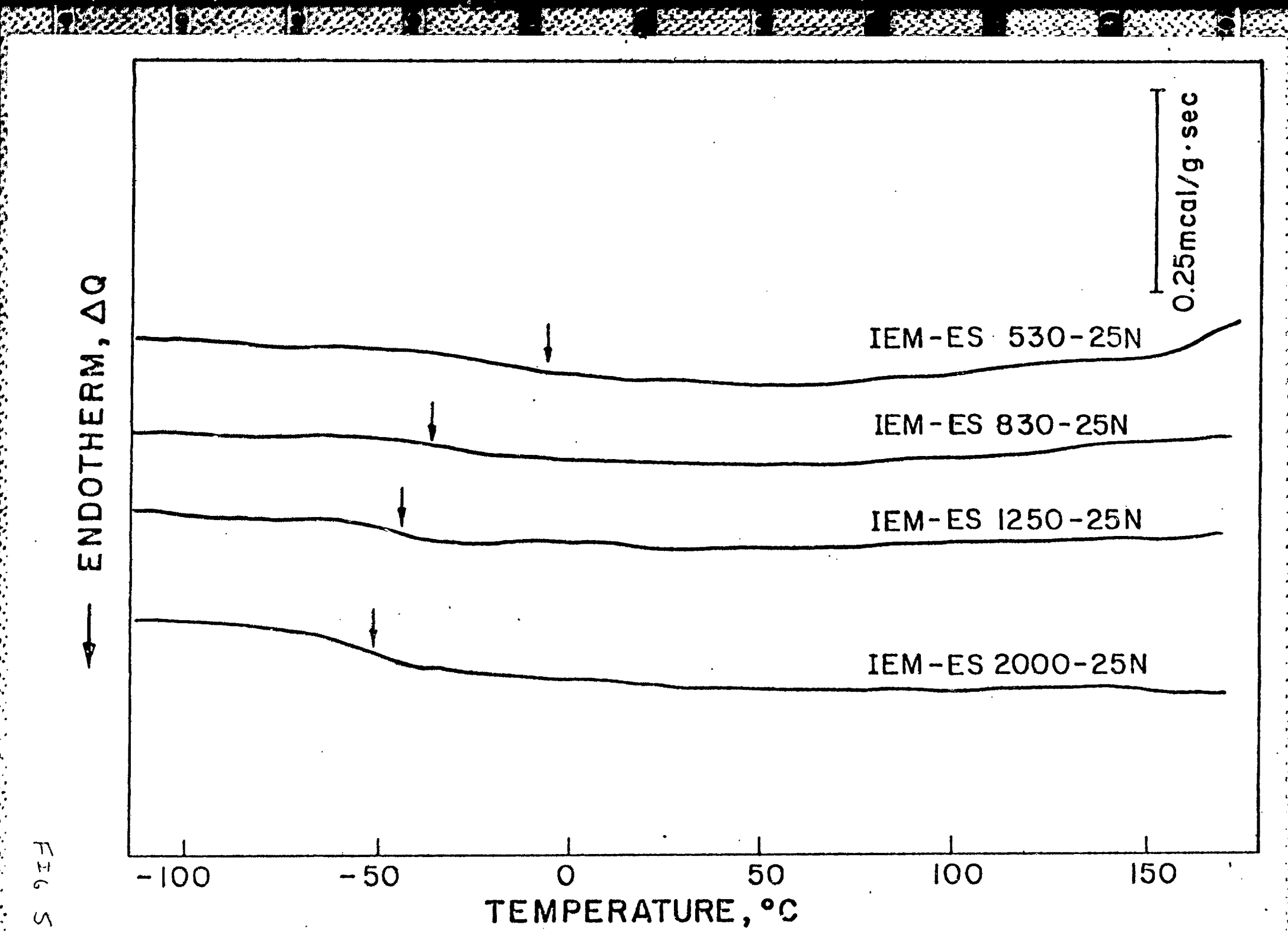
0.25mcal/g·sec
IEM-ES 530-25N
IEM-ES 830-25N
IEM-ES 1250-25N
IEM-ES 2000-25N
ENDOTHERM, ΔQ
-100
-50
0
50
100
150
TEMPERATURE, °C

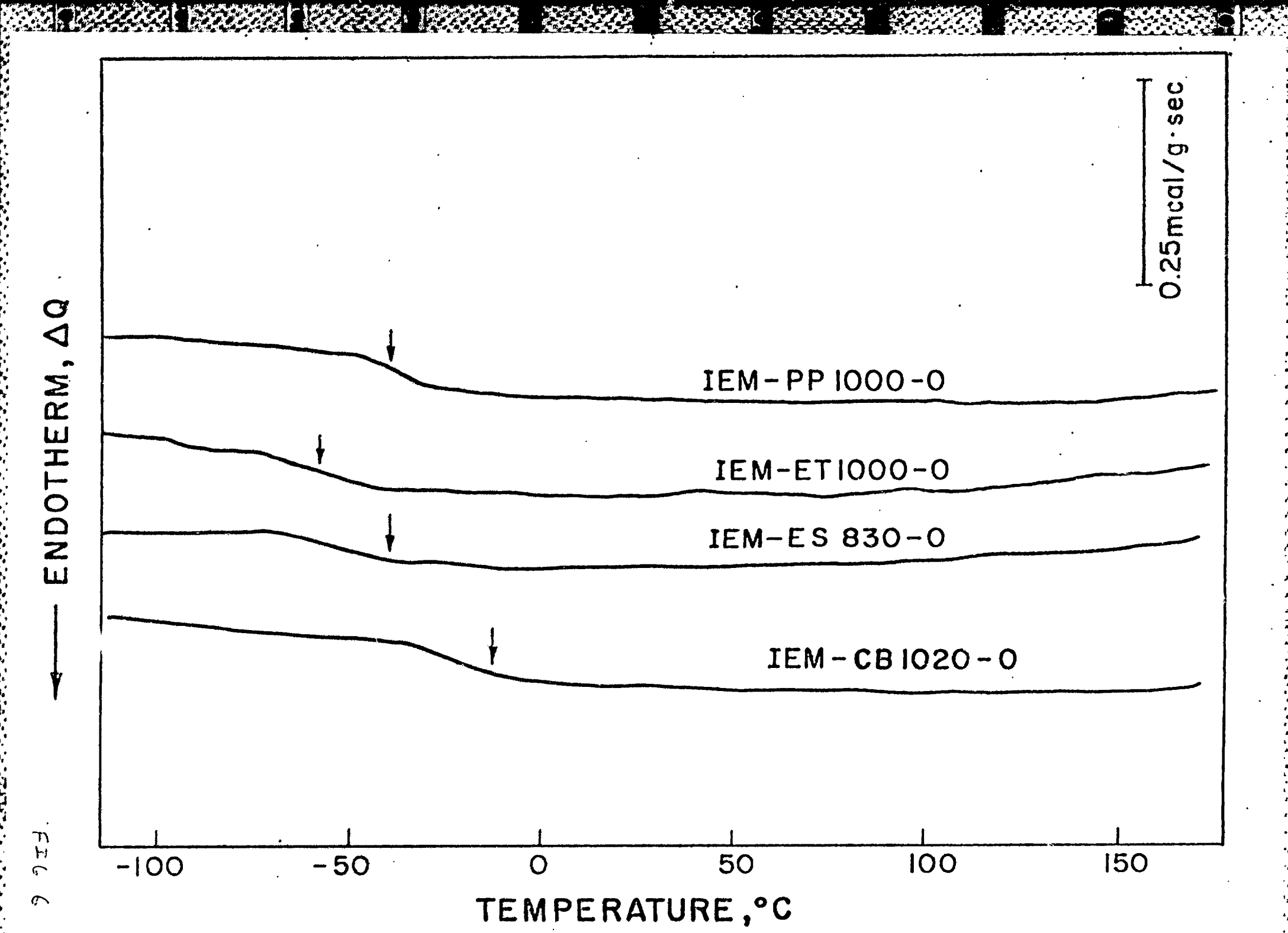
0.25mcal/g·sec
IEM-PP1000-0
IEM-ET1000-0
IEM-ES 830-0
IEM-CB1020-0
ENDOTHERM, ΔQ
-100
-50
0
50
100
150
TEMPERATURE, °C

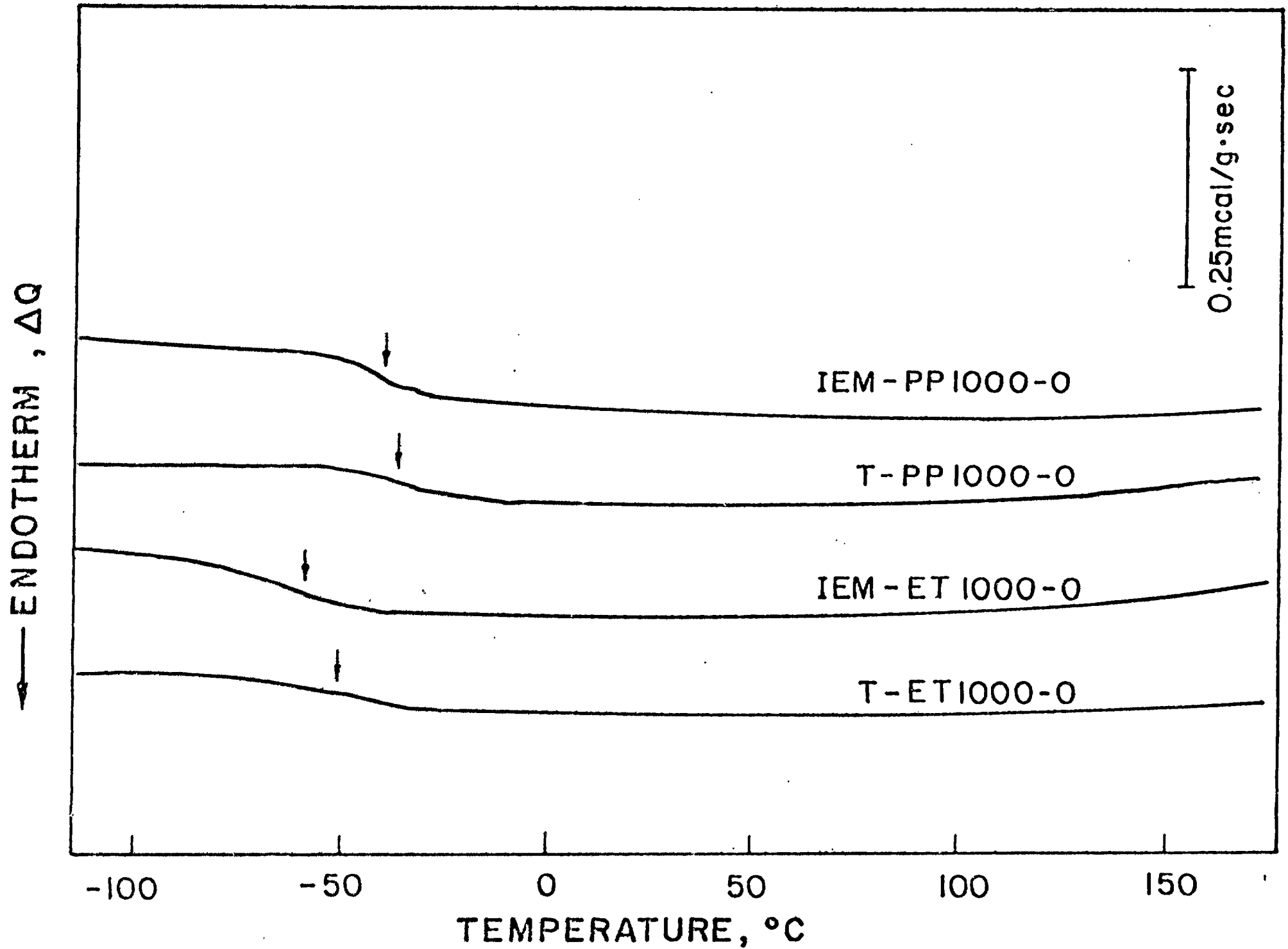
0.25mcal/g·sec
IEM-PP1000-0
T-PP1000-0
IEM-ET1000-0
T-ET1000-0
ENDOTHERM, ΔQ
-100
-50
0
50
100
150
TEMPERATURE, °C

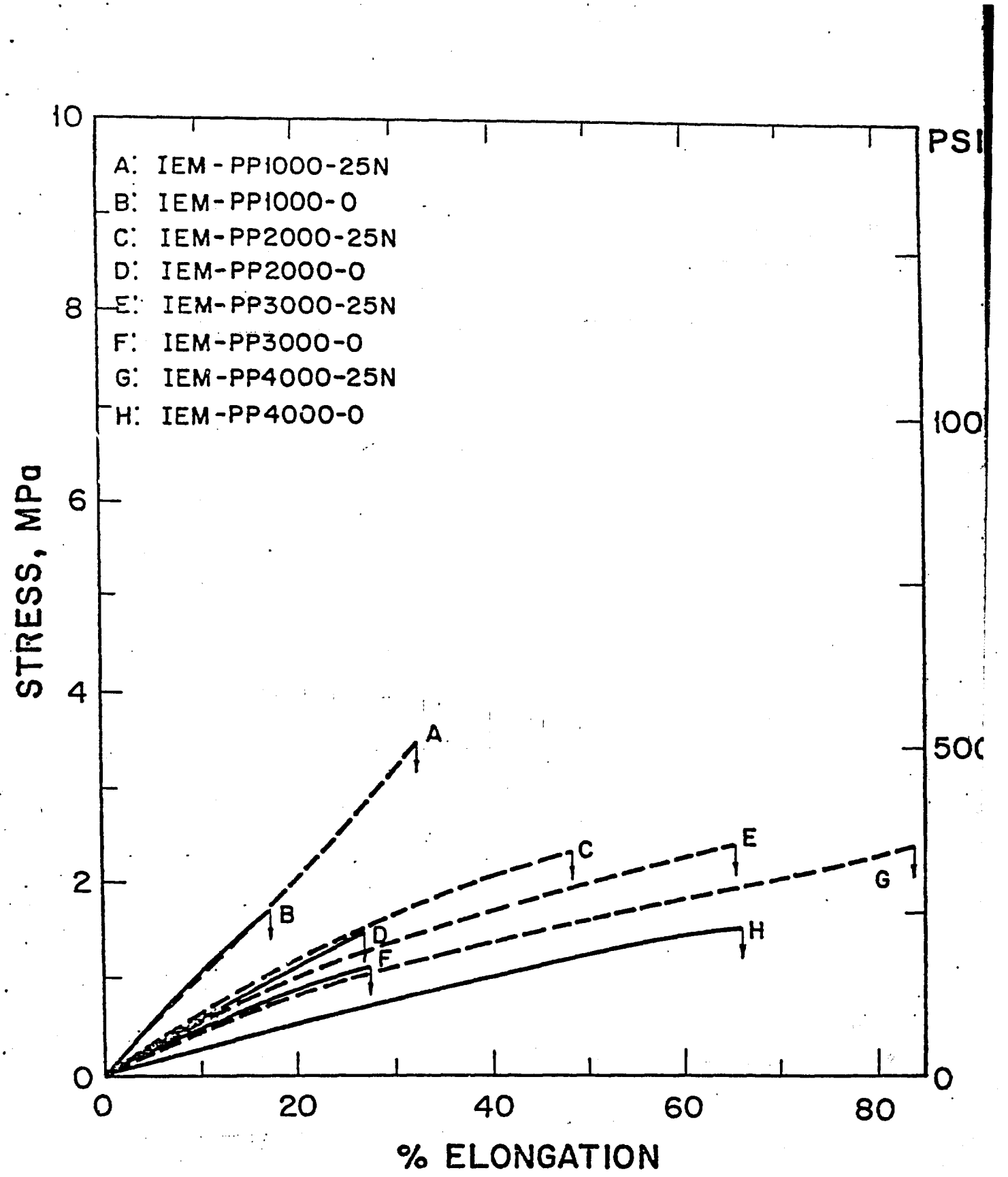
A: IEM-PP1000-25N
B: IEM-PP1000-0
C: IEM-PP2000-25N
D: IEM-PP2000-0
E: IEM-PP3000-25N
F: IEM-PP3000-0
G: IEM-PP4000-25N
H: IEM-PP4000-0
STRESS, MPa
PSI
% ELONGATION
0
2
4
6
8
10
0
20
40
60
80
100
500
A
B
C
D
E
F
G
H

FIG 8

PHYSICAL PROPERTIES OF IEM-PP25N SERIES AS A FUNCTION OF POLYOL MOLECULAR WEIGHT

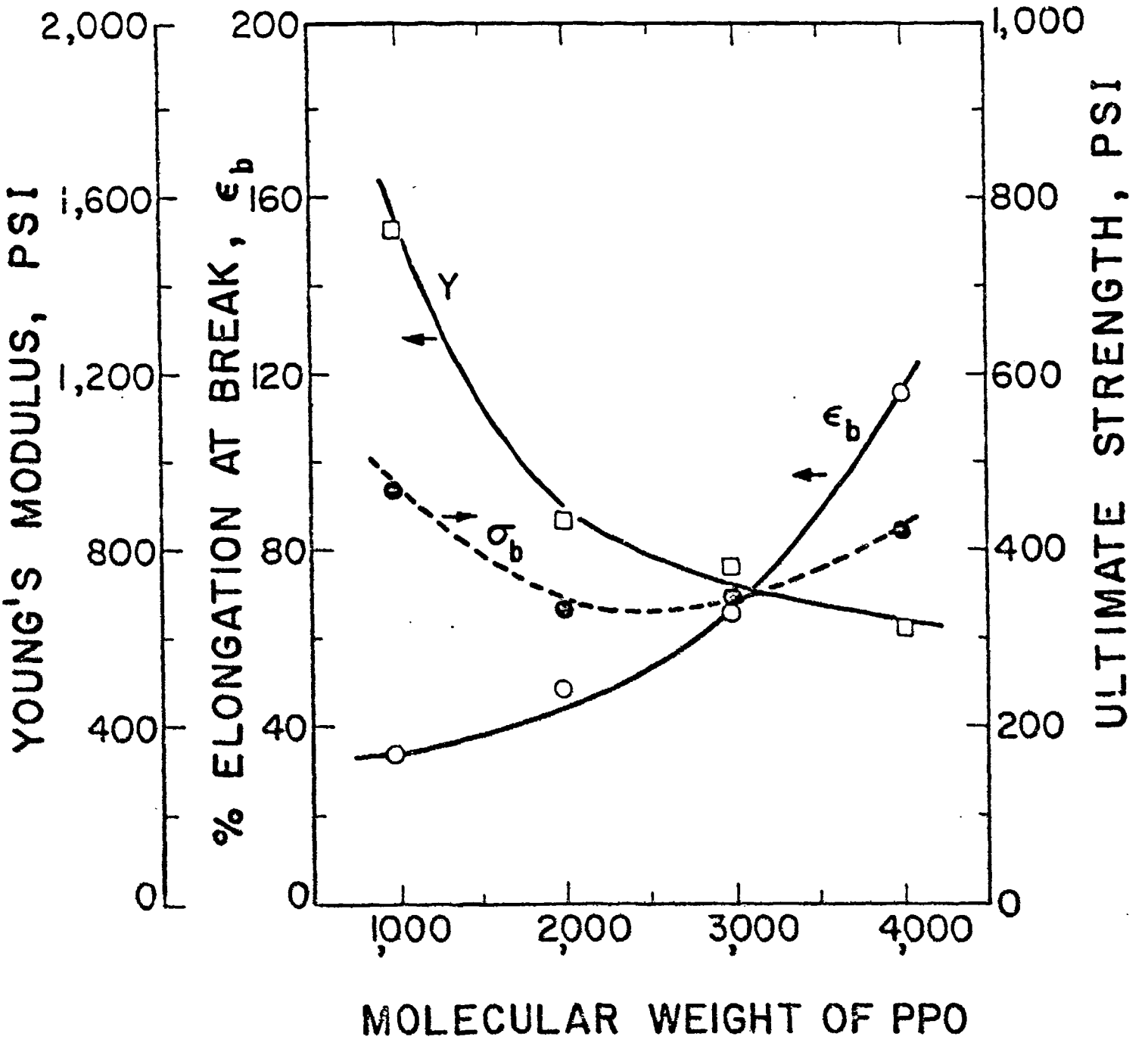

FIG 9

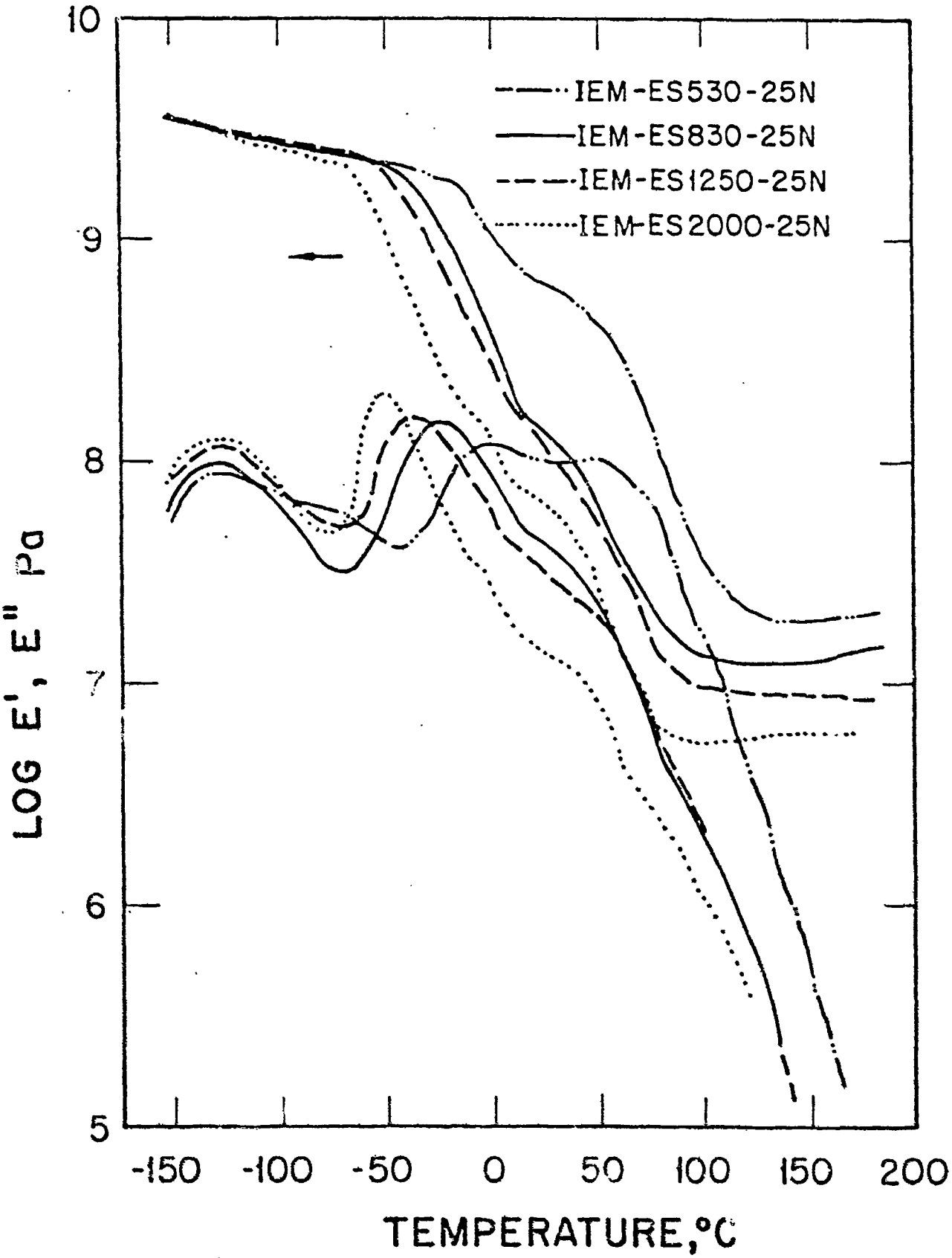
IEM-ES530-25N
IEM-ES830-25N
IEM-ES1250-25N
IEM-ES2000-25N
LOG E', E" Pa
TEMPERATURE,°C
10
9
8
7
6
5
-150
-100
-50
0
50
100
150
200

FIG. 10

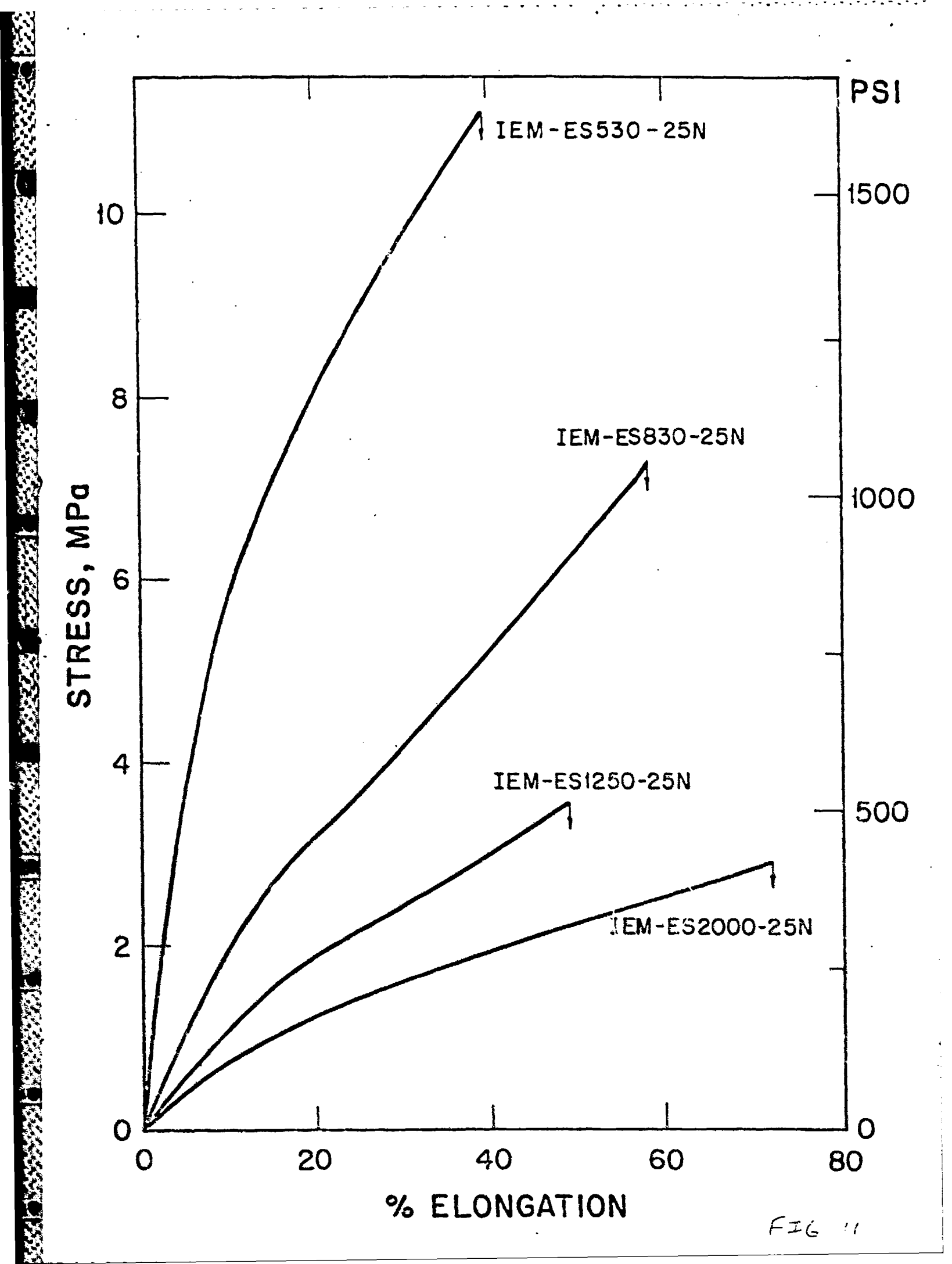
PSI
IEM-ES530-25N
1500
10
8
IEM-ES830-25N
1000
STRESS, MPa
6
4
IEM-ES1250-25N
500
2
IEM-ES2000-25N
0
0
0
20
40
60
80
% ELONGATION

FIG 11

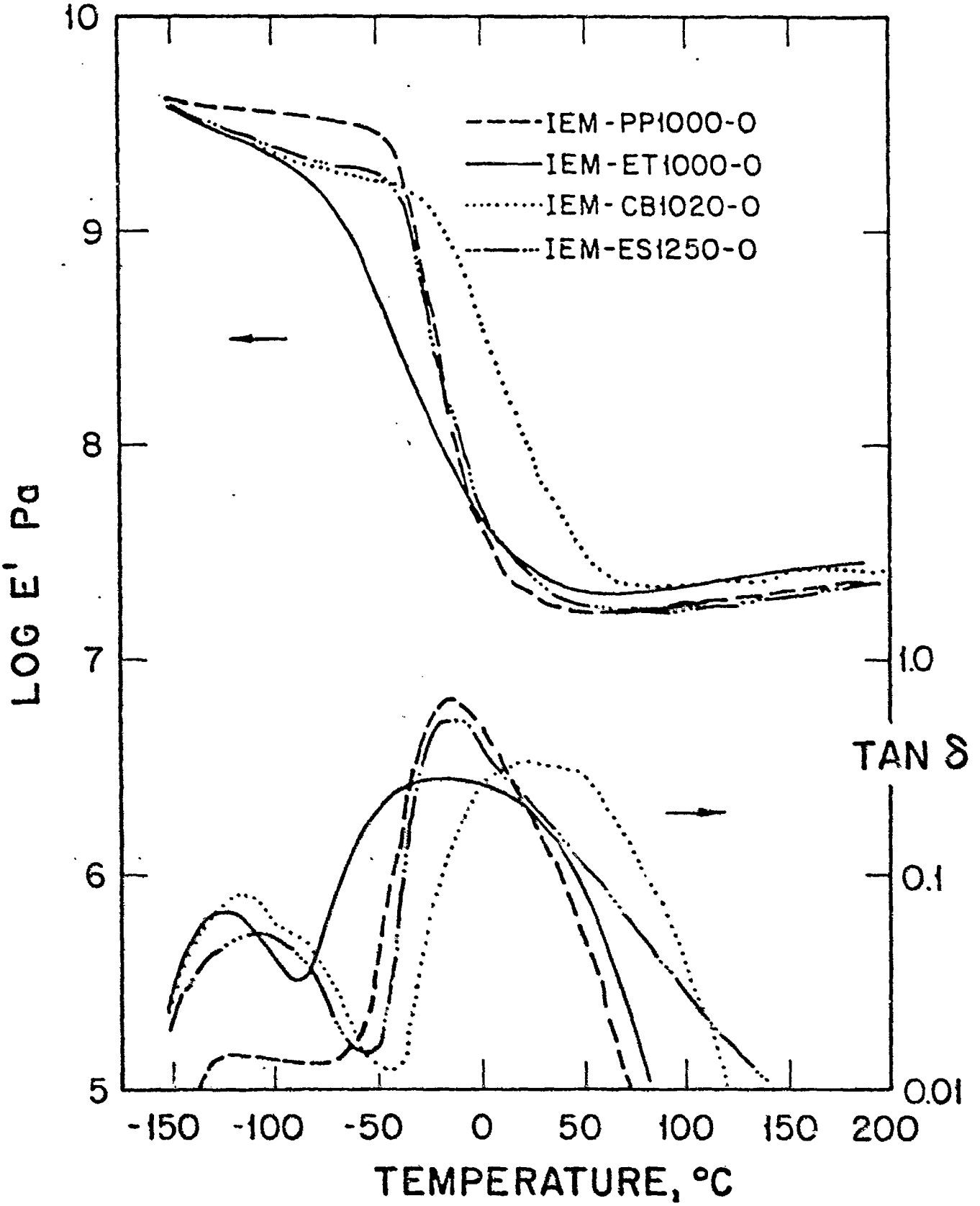
IEM-PP1000-0
IEM-ET1000-0
IEM-CB1020-0
IEM-ES1250-0
LOG E' Pa
TAN δ
TEMPERATURE, °C
10
9
8
7
6
5
1.0
0.1
0.01
-150
-100
-50
0
50
100
150
200

FIG 12

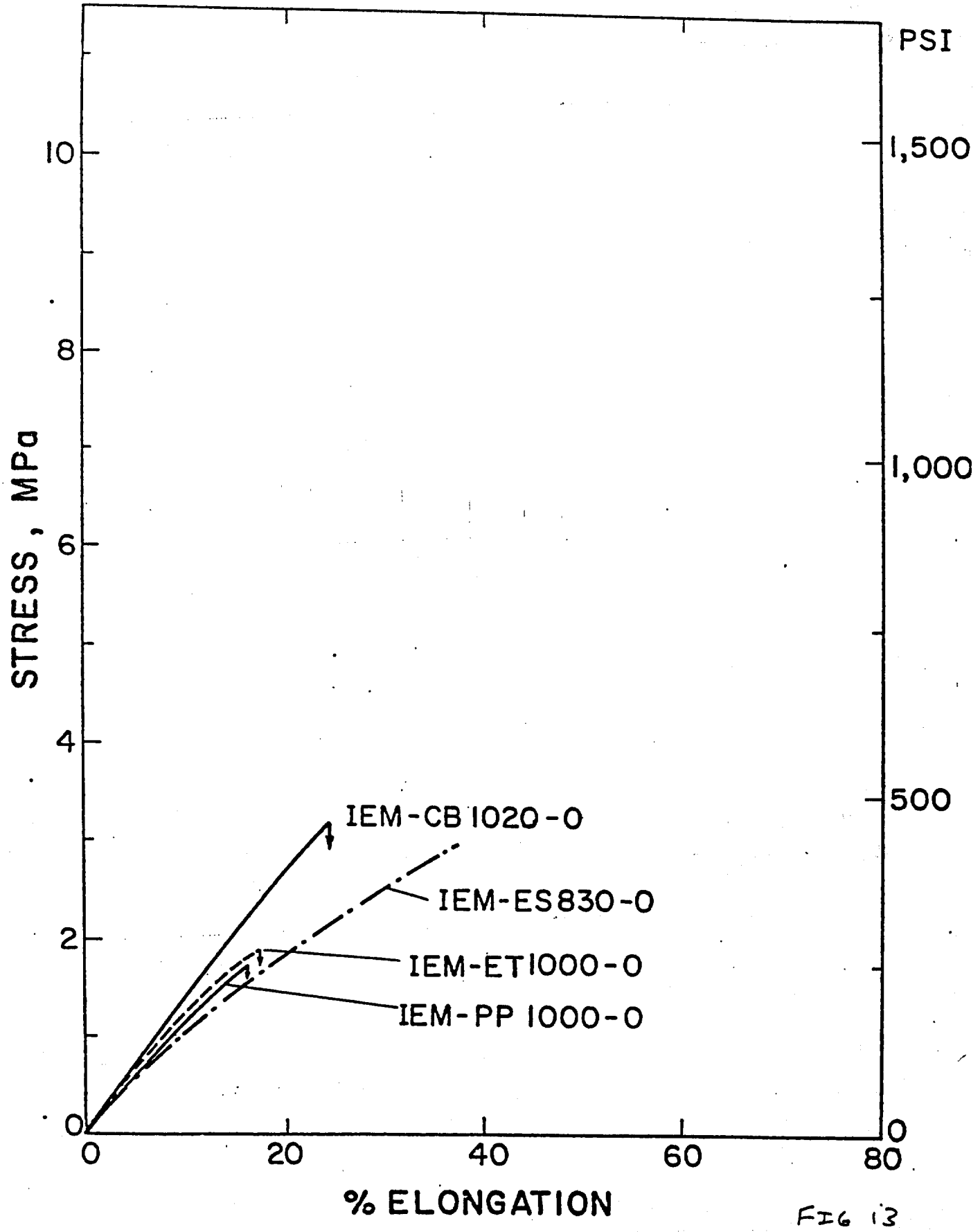
PSI
1,500
1,000
500
0
10
8
6
4
2
0
STRESS, MPa
IEM-CB 1020-0
IEM-ES 830-0
IEM-ET 1000-0
IEM-PP 1000-0
0
20
40
60
80
% ELONGATION

FIG 13

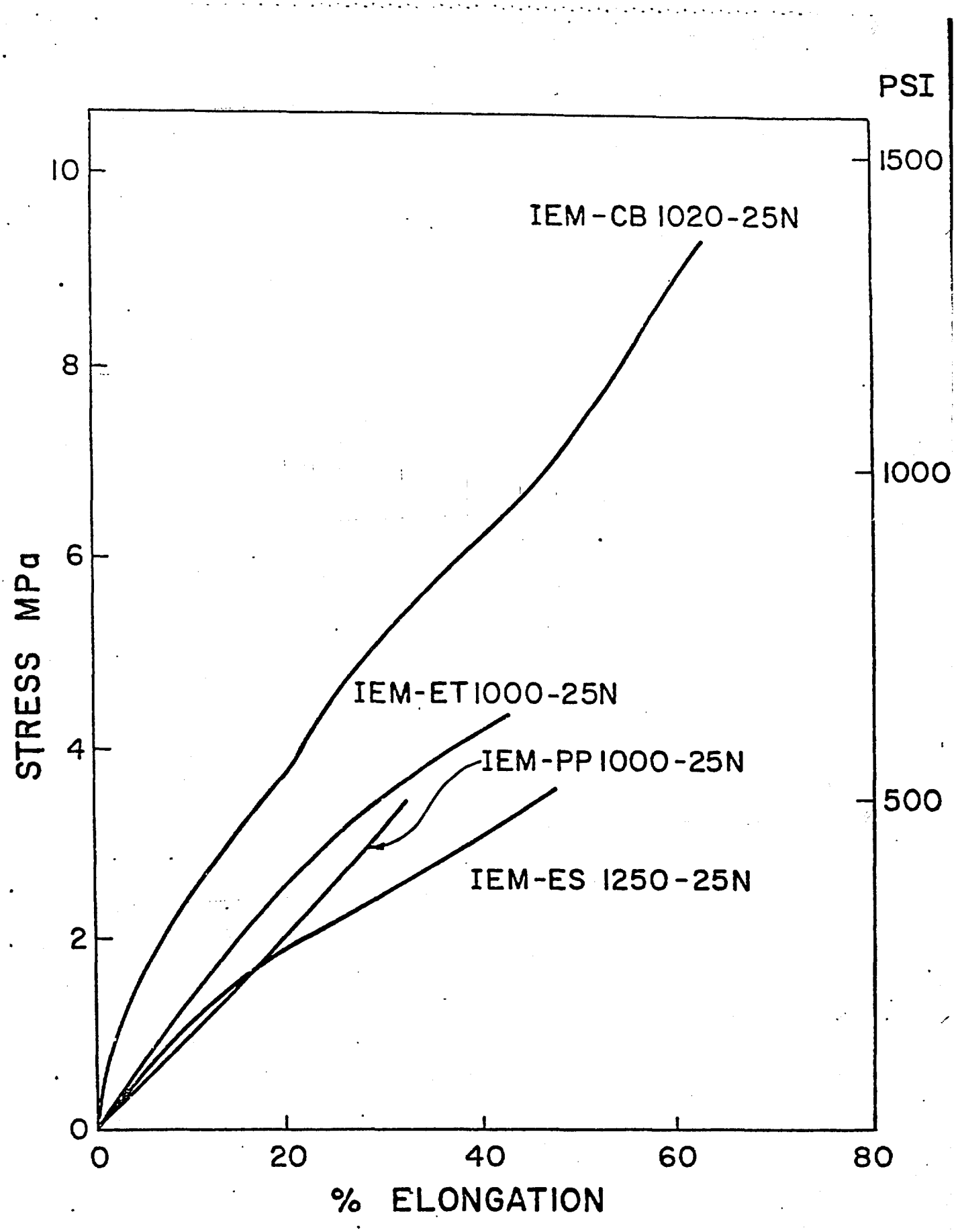
PSI
1500
1000
500
10
8
6
4
2
0
STRESS MPa
IEM-CB 1020-25N
IEM-ET 1000-25N
IEM-PP 1000-25N
IEM-ES 1250-25N
0
20
40
60
80
% ELONGATION

FIG. 14

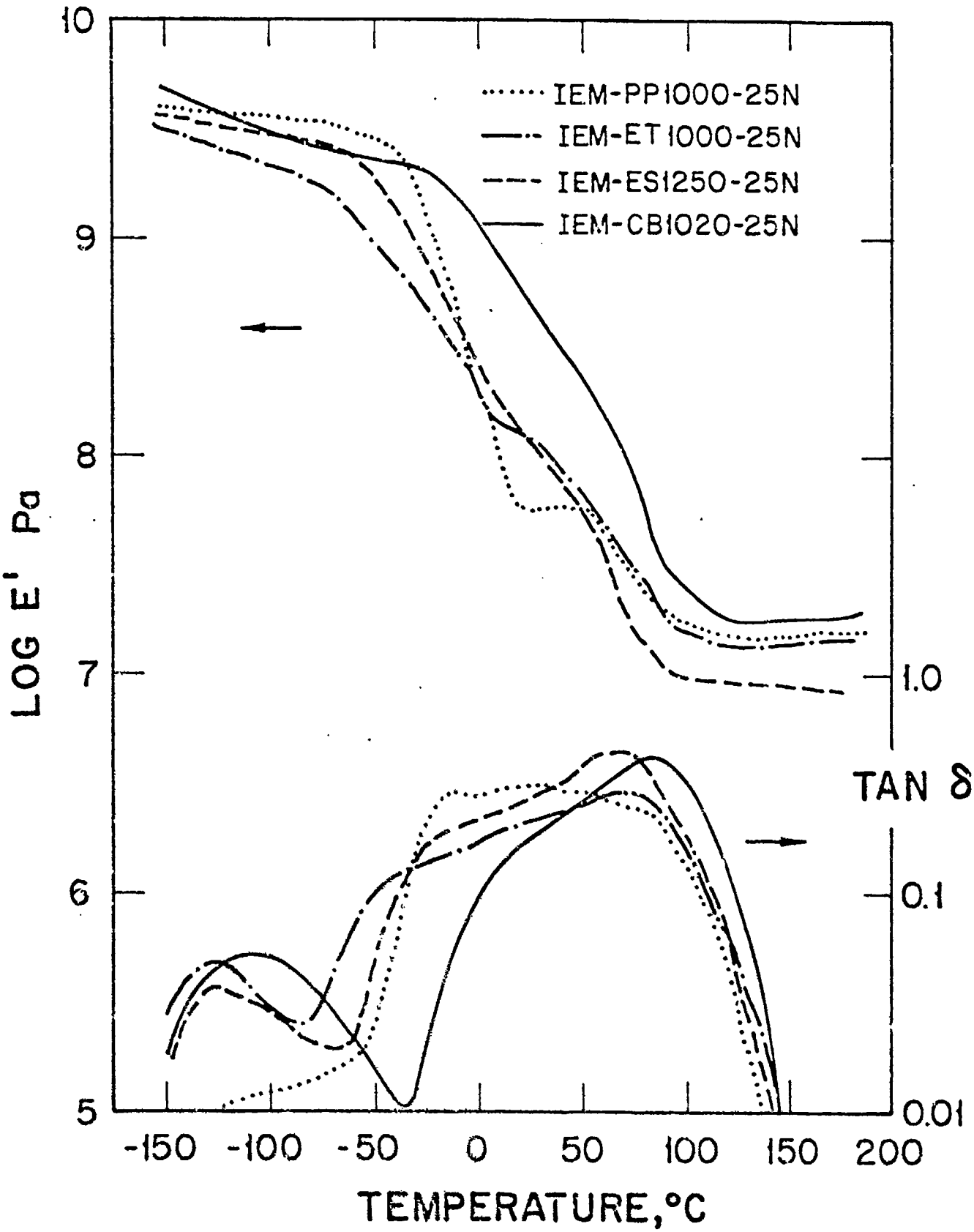
IEM-PP1000-25N
IEM-ET1000-25N
IEM-ES1250-25N
IEM-CB1020-25N
LOG E' Pa
TAN δ
TEMPERATURE, °C
10
9
8
7
6
5
1.0
0.1
0.01
-150
-100
-50
0
50
100
150
200

FIG 15

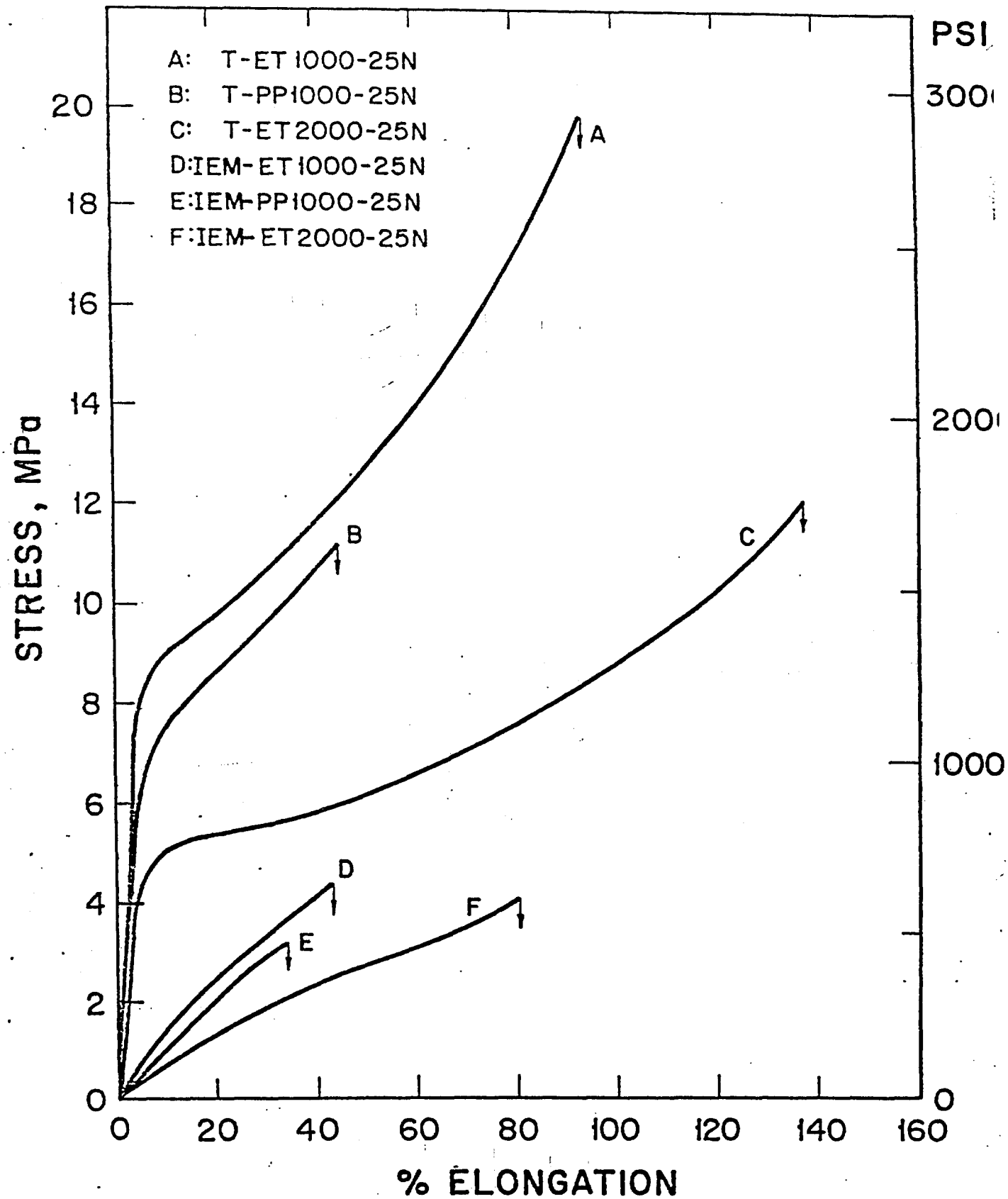
A: T-ET1000-25N
B: T-PP1000-25N
C: T-ET2000-25N
D:IEM-ET1000-25N
E:IEM-PP1000-25N
F:IEM-ET2000-25N
STRESS, MPa
PSI
% ELONGATION
0
2
4
6
8
10
12
14
16
18
20
0
20
40
60
80
100
120
140
160
1000
2000
3000

FIG 16

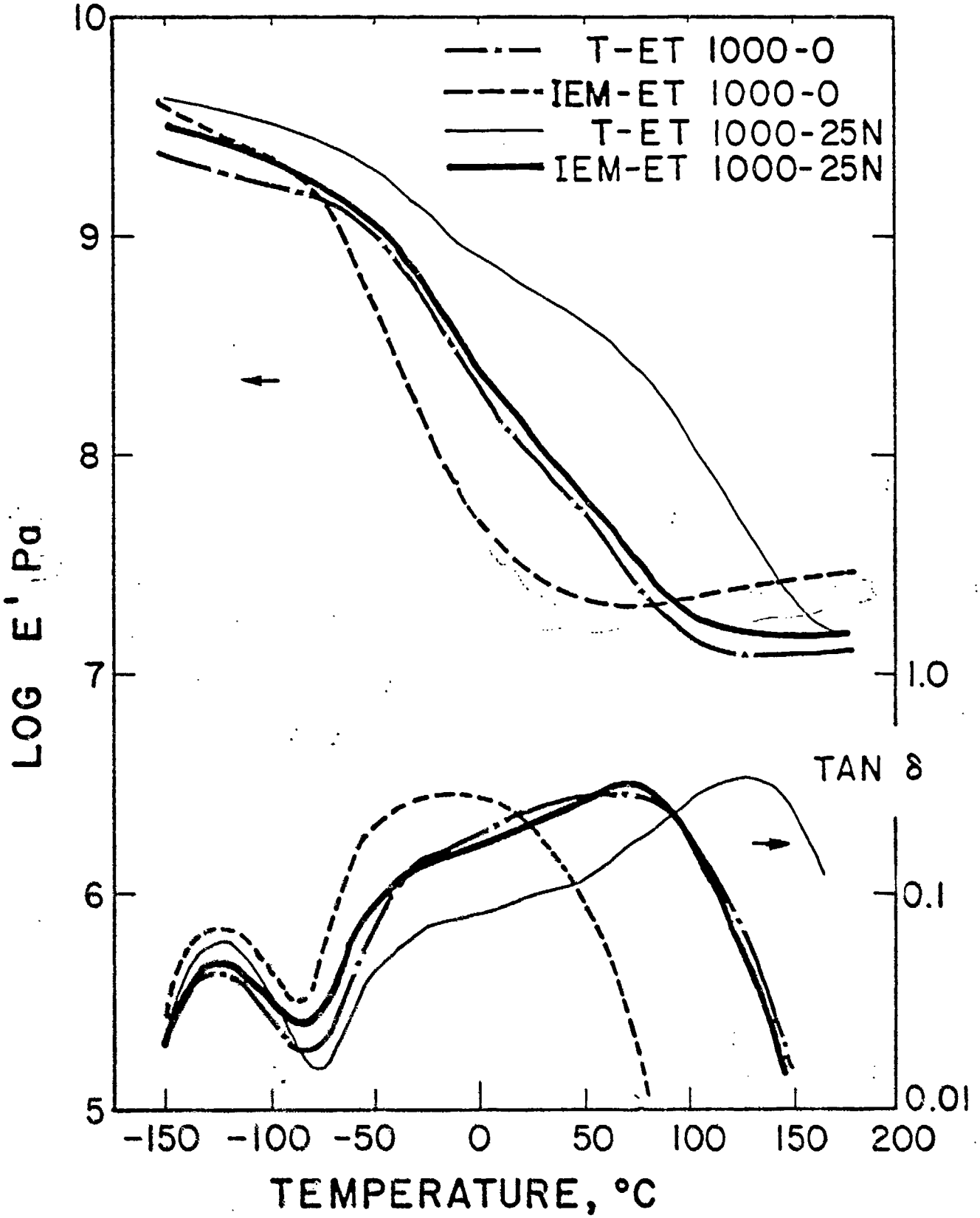
T-ET 1000-0
IEM-ET 1000-0
T-ET 1000-25N
IEM-ET 1000-25N
LOG E' Pa
TAN δ
10
9
8
7
6
5
1.0
0.1
0.01
-150 -100 -50 0 50 100 150 200
TEMPERATURE, °C

DL/413/83/01
GEN/413-2

TECHNICAL REPORT DISTRIBUTION LIST, GEN

	No. Copies
Office of Naval Research Attn: Code 413 800 N. Quincy Street Arlington, Virginia 22217	2
ONR Pasadena Detachment Attn: Dr. R. J. Marcus 1030 East Green Street Pasadena, California 91106	1
Commander, Naval Air Systems Command Attn: Code 310C (H. Rosenwasser) Washington, D.C. 20360	1
Naval Civil Engineering Laboratory Attn: Dr. R. W. Drisko Port Hueneme, California 93401	1
Superintendent Chemistry Division, Code 6100 Naval Research Laboratory Washington, D.C. 20375	1
Defense Technical Information Center Building 5, Cameron Station Alexandria, Virginia 22314	12
DTNSRDC Attn: Dr. G. Bosmajian Applied Chemistry Division Annapolis, Maryland 21401	1
Naval Ocean Systems Center Attn: Dr. S. Yamamoto Marine Sciences Division San Diego, California 91232	1
Naval Ocean Systems Center Attn: Technical Library San Diego, California 92152	1
Naval Weapons Center Attn: Dr. A. B. Amster Chemistry Division China Lake, California 93555	1
Scientific Advisor Commandant of the Marine Corps Code RD-1 Washington, D.C. 20380	1
Dean William Tolles Naval Postgraduate School Monterey, California 93940	1
U.S. Army Research Office Attn: CRD-AA-IP P.O. Box 12211 Research Triangle Park, NC 27709	1
Mr. Vincent Schaper DTNSRDC Code 2830 Annapolis, Maryland 21402	1
Mr. John Boyle Materials Branch Naval Ship Engineering Center Philadelphia, Pennsylvania 19112	1
Mr. A. M. Anzalone Administrative Librarian PLASTEC/ARRADCOM Bldg 3401 Dover, New Jersey 07801	1

TECHNICAL REPORT DISTRIBUTION LIST, 356B

Dr. C. L. Schilling
Union Carbide Corporation
Chemical and Plastics
Tarrytown Technical Center
Tarrytown, New York 10591

Dr. A. G. MacDiarmid
Department of Chemistry
University of Pennsylvania
Philadelphia, Pensylvania 19174

Dr. E. Fischer, Code 2853
Naval Ship Research and
Development Center
Annapolis, Maryland 21402

Dr. H. Allcock
Department of Chemistry
Pennsylvania State University
University Park, Pennsylvania 16802

Dr. M. Kenney
Department of Chemistry
Case Western University
Cleveland, Ohio 44106

Dr. R. Lenz
Department of Chemistry
University of Massachusetts
Amherst, Massachusetts 01002

Dr. M. David Curtis
Department of Chemistry
University of Michigan
Ann Arbor, Michigan 48105

NASA-Lewis Research Center
Attn: Dr. T. T. Serafini, MS 49-1
21000 Brookpark Road
Cleveland, Ohio 44135

Dr. J. Griffith
Naval Research Laboratory
Chemistry Section, Code 6120
Washington, D.C. 20375

Professor G. Wnek
Department of Materials Science
and Engineering
Massachusetts Institute of Technology
Cambridge, Massachusetts 02139

Dr. R. Soulen
Contract Research Department
Pennwalt Corporation
900 First Avenue
King of Prussia, Pennsylvania 1940[illegible]

Dr. G. Goodman
Globe-Union Incorporated
5757 North Green Bay Avenue
Milwaukee, Wisconsin 53201

Dr. Martin H. Kaufman
Code 38506
Naval Weapons Center
China Lake, California 93555

Dr. C. Allen
Department of Chemistry
University of Vermont
Burlington, Vermont 05401

Professor R. Drago
Department of Chemistry
University of Florida
Gainesville, Florida 32611

Dr. D. L. Venezky
Code 6130
Naval Research Laboratory
Washington, D.C. 20375

Professor T. Katz
Department of Chemistry
Columbia University
New York, New York 10027

Professor James Chien
Department of Chemistry
University of Massachusetts
Amherst, Massachusetts 01002

Professor J. Salamone
Department of Chemistry
University of Lowell
Lowell, Massachusetts 01854

CAPT J. J. Auborn, USNR
AT&T Bell Laboratories
Room 6F-211
600 Mountain Avenue
Murray Hill, New Jersey 07974

DL/413/83/01
356B/413-2

TECHNICAL REPORT DISTRIBUTION LIST, 356B

Professor D. Grubb
Department of Materials Science
and Engineering
Cornell University
Ithaca, New York 14853

Professor T. Marks
Department of Chemistry
Northwestern University
Evanston, Illinois 60201

Professor C. Chung
Department of Materials Engineering
Rensselaer Polytechnic Institute
Troy, New York 12181

Professor Malcolm B. Polk
Department of Chemistry
Atlanta University
Atlanta, Georgia 30314

Dr. D. B. Cotts
SRI International
333 Ravenswood Avenue
Menlo Park, California 94205

Dr. Kurt Baum
Fluorochem, Inc.
680 S. Ayon Avenue
Azuza, California 91702

Professor H. Hall
Department of Chemistry
University of Arizona
Tucson, Arizona 85721

Professor G. Whitesides
Department of Chemistry
Harvard University
Cambridge, Massachusetts 02138

Professor H. Ishida
Department of Macromolecular Science
Case Western University
Cleveland, Ohio 44106

Dr. K. Paciorek
Ultrasystems, Inc.
P.O. Box 19605
Irvine, California 92715

Professor D. Seyferth
Department of Chemistry
Massachusetts Institute of Technology
Cambridge, Massachusetts 02139

Dr. G. Bryan Street
IBM Research Laboratory, K32/281
San Jose, California 95193